

## **(Pro)renin Receptor Inhibition Reprograms Hepatic Lipid Metabolism and Protects Mice From Diet-Induced Obesity and Hepatosteatosis**

Liwei Ren,\* Yuan Sun,\* Hong Lu, Dien Ye, Lijuan Han, Na Wang, Alan Daugherty, Furong Li, Miaomiao Wang, Fengting Su, Wenjun Tao, Jie Sun, Noam Zelcer, Adam E. Mullick, A.H. Jan Danser, Yizhou Jiang, Yongcheng He, Xiongzong Ruan#, Xifeng Lu#

From the AstraZeneca-Shenzhen University Joint Institute of Nephrology, Department of Physiology, Shenzhen University Health Science Center, Shenzhen University, China (L.R., Y.S., D.Y., L.H., N.W., M.W., F.S., W.T., J.S., X.R., X.L.); Translational Medicine Collaborative Innovation Center, The Second Clinical Medical College (Shenzhen People's Hospital) of Jinan University, Shenzhen, China (L.R., Y.S., F.L., X.L.); Division of Pharmacology and Vascular Medicine, Department of Internal Medicine, Erasmus Medical Center, Rotterdam University, The Netherlands (L.R., Y.S., A.H.J.D.); Saha Cardiovascular Research Center and Department of Physiology, University of Kentucky, Lexington (H.L., A.D.); Department of Medical Biochemistry, Academic Medical Center, University of Amsterdam, The Netherlands (N.Z.); Ionis Pharmaceuticals, Inc, Carlsbad, CA (A.E.M.); Institute for Advanced Study, Shenzhen University, China (Y.J.); The First Affiliated Hospital of Shenzhen University, China (Y.H.); and John Moorhead Laboratory, Center for Nephrology, University College London, United Kingdom (X.R.).

\*These authors contributed equally to this article.

#: corresponding authors.

Correspondence to Xifeng Lu, PhD, MSc, Shenzhen University Health Science Center, Room 517, Shenzhen University, Nanhai Ave 3688, 518060 Shenzhen, China, E-mail x.lu@szu.edu.cn; or Xiongzong Ruan, PhD, E-mail xiongzruan@gmail.com.

**Rationale:** An elevated level of plasma LDL (low-density lipoprotein) is an established risk factor for cardiovascular disease. Recently, we reported that the (pro)renin receptor ([P]RR) regulates LDL metabolism in vitro via the LDLR (LDL receptor) and SORT1 (sortilin-1), independently of the renin–angiotensin system.

**Objectives:** To investigate the physiological role of (P)RR in lipid metabolism in vivo.

**Methods and Results:** We used N-acetylgalactosamine modified antisense oligonucleotides to specifically inhibit hepatic (P)RR expression in C57BL/6 mice and studied the consequences this has on lipid metabolism. In line with our earlier report, hepatic (P)RR silencing increased plasma LDL-C (LDL cholesterol). Unexpectedly, this also resulted in markedly reduced plasma triglycerides in a SORT1-independent manner in C57BL/6 mice fed a normal- or high-fat diet. In LDLR-deficient mice, hepatic (P)RR inhibition reduced both plasma cholesterol and triglycerides, in a diet-independent manner. Mechanistically, we found that (P)RR inhibition decreased protein abundance of ACC (acetyl-CoA carboxylase) and PDH (pyruvate dehydrogenase). This alteration reprograms hepatic metabolism, leading to reduced lipid synthesis and increased fatty acid oxidation. As a result, hepatic (P)RR inhibition attenuated diet-induced obesity and hepatosteatosis.

**Conclusions:** Collectively, our study suggests that (P)RR plays a key role in energy homeostasis and regulation of plasma lipids by integrating hepatic glucose and lipid metabolism.

**Key Words:** dyslipidemia, hypercholesterolemia, hypertriglyceridemia, liver renin-angiotensin system, vacuolar H<sup>+</sup>-ATPase

### **Introduction:**

Elevated plasma LDL (low-density lipoprotein) levels are a major risk factor for developing atherosclerosis and ensuing ischemic cardiovascular disease, a leading cause of worldwide death. LDL, which is derived by peripheral lipolysis of VLDL (very-low-density lipoprotein), is primarily cleared from the circulation in the liver via the LDLR (LDL receptor) pathway<sup>1,2</sup>. Hence, plasma LDL levels are determined by the dynamic balance between hepatic VLDL secretion and LDL clearance.

VLDL particles are formed by lipidation of apo (apolipoprotein) B100, the core protein of VLDL, in the endoplasmic reticulum and Golgi apparatus<sup>3</sup>. The assembly of VLDL particles depends on apo B100 production and cellular availability of triglycerides. Accordingly, genetic mutations in apo B100 are associated with altered VLDL secretion and plasma LDL levels<sup>4-6</sup>. Overexpression of apo B100 results in increased VLDL secretion and plasma LDL levels in rabbits<sup>7</sup>. Similarly, the activity of enzymes involved in de novo lipid biosynthesis also affects VLDL assembly and secretion<sup>8,9</sup>. For example, impaired loading of triglycerides into nascent VLDL particles, caused by mutations in the MTP (microsomal triglyceride carrier protein), results in defective VLDL secretion<sup>10</sup>. Disturbed LDL clearance can increase plasma LDL levels and risk for cardiovascular diseases. In line with this, loss-of function LDLR mutations are associated with elevated plasma LDL levels and cardiovascular risk<sup>11-13</sup>. Recently, GWAS studies have identified single-nucleotide polymorphisms mapping to 1p13.3 that strongly associated with plasma LDL levels and coronary heart disease<sup>14-19</sup>. Subsequent mechanistic studies revealed that SORT1 (sortilin-1), located within the 1p13.3 region, is a novel regulator of LDL metabolism<sup>20-22</sup>. Overexpression of SORT1 increases LDL clearance and decreases plasma LDL levels<sup>16,21,22</sup>, whereas SORT1 deficiency reduces cellular LDL uptake in vitro and LDL clearance in vivo<sup>22,23</sup>. In addition, SORT1 also plays a role in VLDL secretion. Overexpressing SORT1 promotes ApoB degradation via an endolysosome-dependent route and hence reduces VLDL secretion and plasma triglyceride levels<sup>22</sup>. Controversially, mice deficient for SORT1 also display reduced VLDL secretion and triglyceride levels<sup>20,22</sup>. These opposing results highlight the complex, and not yet fully elucidated, role of SORT1 in lipoprotein metabolism. The (pro)renin receptor ([P]RR) interacts with renin/prorenin (denoted as [pro]renin) at supraphysiological concentrations that are even several orders of magnitude higher than (patho)physiological concentrations, questioning the physiological relevance of the (P)RR-(pro)renin interaction<sup>24,25</sup>. Recently, the (P)RR was reported to play a role in Wnt/ $\beta$ -catenin signaling pathway, vacuolar H<sup>+</sup>-ATPase integrity, and T-cell

development, independently of (pro)renin<sup>26–30</sup>. Moreover, we have recently identified the (P)RR as a SORT1-interacting protein<sup>31</sup> and demonstrated that silencing (P)RR expression in hepatocytes in vitro reduces protein abundance of SORT1 and LDLR post-transcriptionally, and consequently cellular LDL uptake. To understand the role of the (P)RR in lipoprotein metabolism in vivo, we studied here the consequence of hepatic (P)RR silencing on lipoprotein metabolism. We report that hepatic loss of (P)RR in mice results in a SORT1-dependent increase in plasma LDL levels, but unexpectedly also in a reduction in plasma triglycerides that was SORT1 independent that resulted from altered metabolic reprogramming of hepatocytes. Our study thus highlights hepatic (P)RR as a crucial regulator of energy and lipid metabolism.

## **Results:**

### **Inhibiting Hepatic (P)RR Reduced Both Hepatic LDL Clearance and VLDL Secretion**

We have previously reported that (P)RR inhibition attenuates cellular LDL uptake by reducing LDLR and SORT1 protein abundance in hepatocytes<sup>31</sup>. To understand the role of hepatic (P)RR in lipoprotein metabolism in vivo, we used N-acetylgalactosamine modified antisense oligonucleotides to inhibit hepatic (P)RR expression. At a dose of 3.0 mg kg<sup>-1</sup> wk<sup>-1</sup>, N-acetylgalactosamine (P)RR antisense oligonucleotide (G-[P]RR) potently reduced (P)RR expression in liver, but had no effects on its expression in other major organs, including heart, kidney, intestine, spleen, and different adipose tissues (Online Figure IA and IC through IF). In line with our previous report, inhibiting the (P)RR specifically reduced hepatic LDLR and SORT1 protein levels without affecting their transcript levels (Online Figure IB). As a result of reduced hepatic LDLR and SORT1 protein abundance, (P)RR inhibition elevated plasma cholesterol levels in normal diet (ND)-fed mice, primarily by increasing cholesterol content in IDL (intermediate-density lipoprotein)/LDL fractions (Figure 1A and 1B). Because plasma LDL-C concentrations reflect the balance between hepatic LDL clearance and VLDL secretion, we then investigated the effects of (P)RR inhibition on LDL clearance and hepatic VLDL output. In line with decreased LDLR and SORT1, inhibiting hepatic (P)RR led to attenuated clearance of injected Dil-labeled human LDL (Figure 1C). Unexpectedly, (P)RR inhibition also significantly decreased plasma triglyceride concentrations (Figure 1D), a finding that could be attributed to reduced hepatic VLDL secretion (Figure 1E).

We then asked if silencing (P)RR in hepatocytes could aggravate hypercholesterolemia in C57BL/6 mice fed a high-fat diet (HFD). Like in ND-fed mice, 1 week after (P)RR inhibition, plasma cholesterol levels were 3- to 4- fold higher than those measured in N-acetylgalactosamine control antisense oligonucleotide (G-control)-injected mice (Figure 2A). This elevation was primarily attributed to a marked increase in cholesterol content in the IDL/LDL fraction (Figure 2B). Notably, (P)RR inhibition also increased cholesterol contents in the VLDL fraction and reduced cholesterol contents in the HDL (high-density lipoprotein)

fraction. Unexpectedly, within 2 weeks, plasma cholesterol levels of G-(P)RR-injected mice were normalized and similar to those in the saline-injected or G-control-injected mice (Figure 2A and 2C; Online Figure IG). This contrasts with the sustained increase in plasma cholesterol levels in C57BL/6 mice fed with ND (Online Figure IH). Nevertheless, (P)RR inhibition in HFD-fed mice reduced hepatic LDL clearance and VLDL secretion (Figure 2D and 2E). Plasma triglycerides and VLDL triglycerides were both lower in G-(P)RR-injected mice when compared with saline or G-control-injected mice (Figure 2F and 2G), thus mimicking the pattern seen under ND feeding. Importantly, plasma LPL (lipoprotein lipase) activity was not affected by hepatic (P)RR inhibition (Figure 2H). This excludes the possibility that increased triglyceride hydrolysis underpins reduced levels of plasma triglycerides in (P)RR-silenced mice.

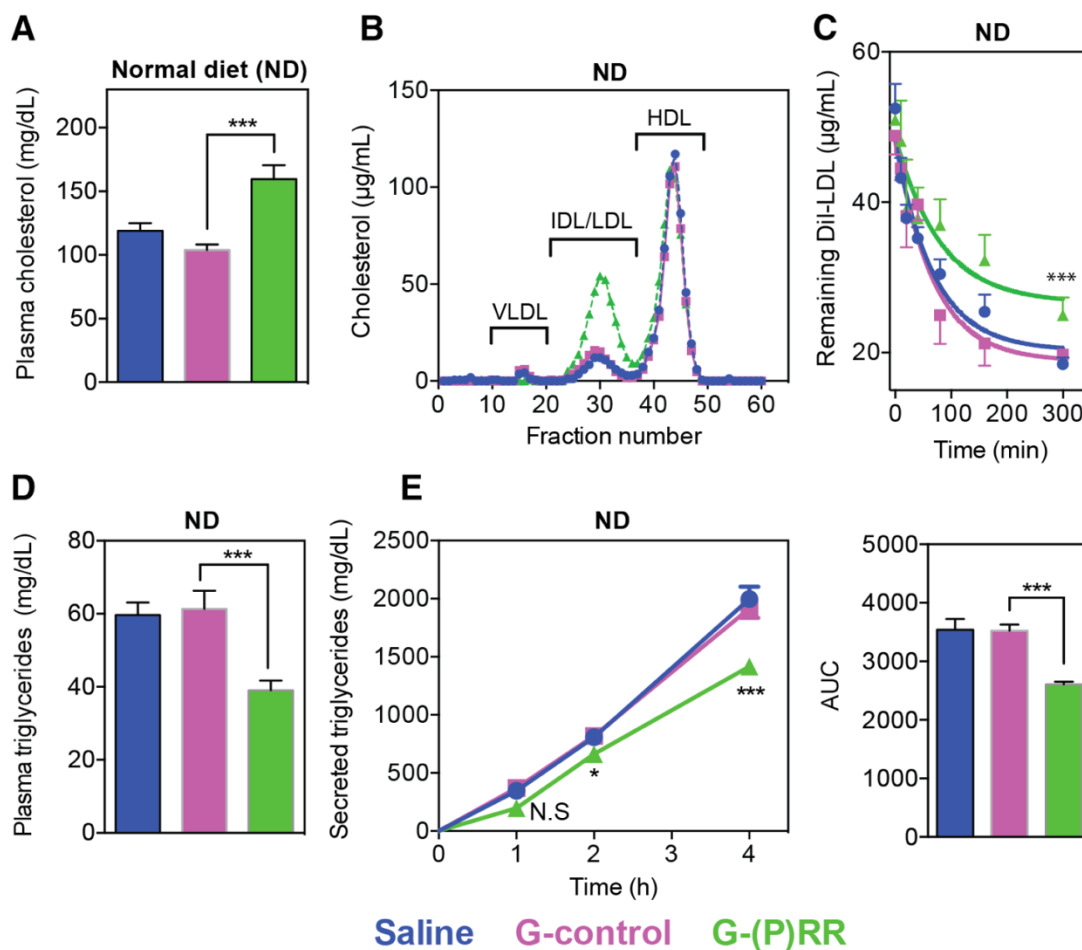


**Figure 1.** Inhibiting hepatic (pro)renin receptor ((P)RR) induces hypercholesterolemia by reducing hepatic LDL (low-density lipoprotein) clearance in normal diet (ND)-fed C57BL/6 mice. Eight-week-old male C57BL/6 mice were injected with either saline (blue), G-control (magenta), or G-(P)RR (green) intraperitoneally. Mice were euthanized after 7 days, and blood samples were collected for (A) determining circulating levels of cholesterol (n=12–18 per group). Each bar and error represent the mean±SEM; \*\*\*P<0.001, or (B) pooled plasma samples were loaded on FPLC (fast protein liquid chromatography) for lipoprotein fractionation analysis, and cholesterol content in each

fraction was determined. C, Seven days after injection, mice (n=6 per group) were injected with 50  $\mu$ g Dil-labeled human LDL. Blood samples were drawn retro-orbitally at the indicated time points, and the Dil-LDL was determined. Each point represents the mean $\pm$ SEM, and the area under curve (AUC) was constructed for each group and used to compare the difference in LDL clearance.\*\*\*P<0.001. D, Blood was collected as in (A) and used to determine plasma triglyceride levels. n=12–18 per group; Each bar and error represent the mean $\pm$ SEM. \*\*\*P<0.001. E, Seven days after injection, mice (n=6 per group) were fasted for 6 hours and injected with Pluronic F127 to inhibit lipoprotein lipase. Blood samples were drawn retro-orbitally at the indicated time points, and the concentration of triglycerides was determined. The mean VLDL (very-low-density lipoprotein) secretion for saline-injected, G-control-injected, or G-(P) RR-injected mice is 474 $\pm$ 16, 460 $\pm$ 14, and 342 $\pm$ 10 mg/dL•h, respectively. The AUC was calculated for individual mice and used to compare the differences in the rate of VLDL secretion. \*\*\*P<0.001; G-control vs G-(P)RR. HDL indicates high-density lipoprotein; and IDL, intermediate-density lipoprotein.

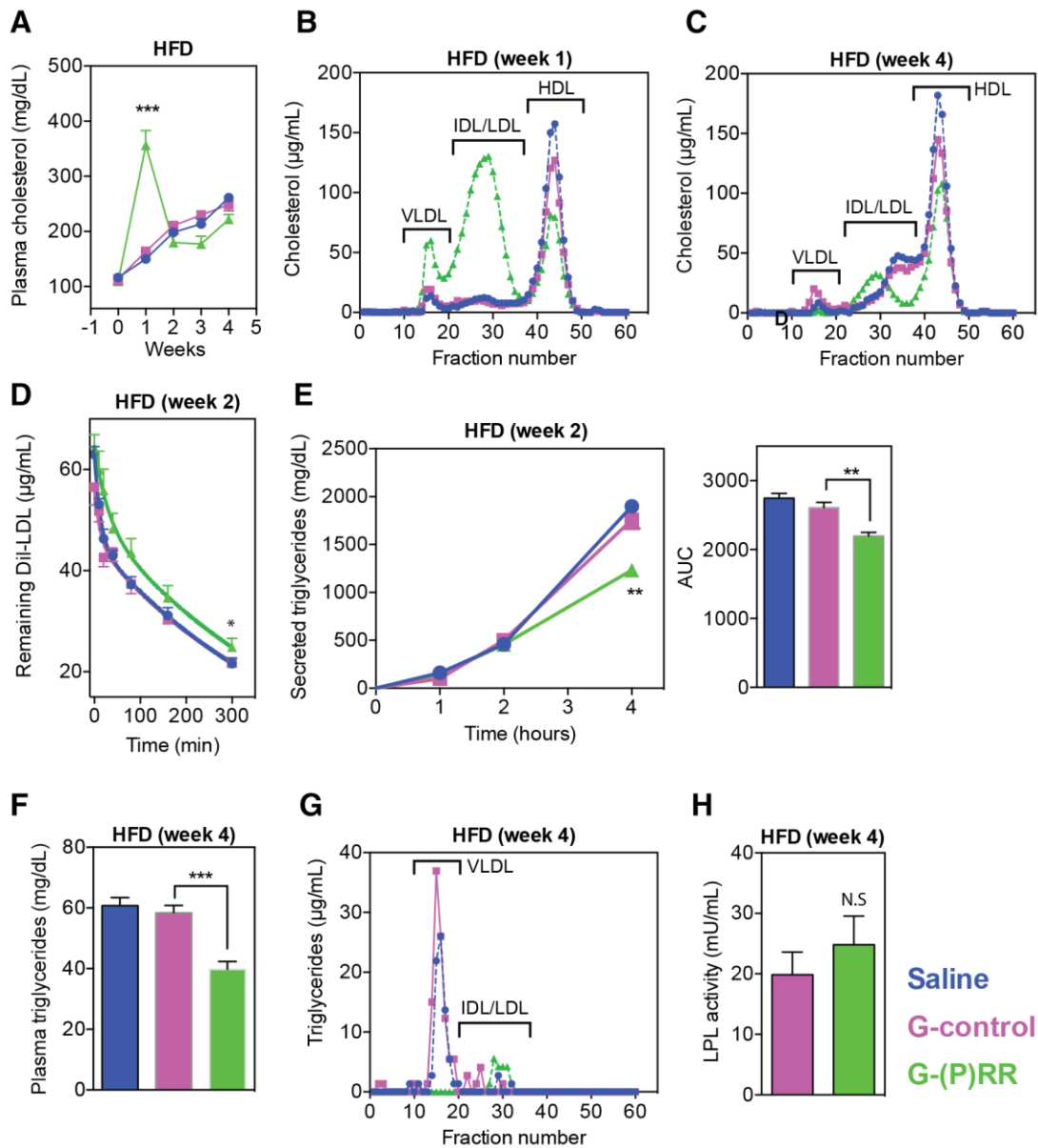


**Figure 2.** Inhibiting hepatic (pro)renin receptor ((P)RR) does not result in hypercholesterolemia in high-fat diet (HFD)–fed C57BL/6 mice. Eight-week-old male C57BL/6 mice were injected with either saline (blue), G-control (magenta), or G-(P)RR (green), and fed an HFD for 4 weeks. A, Plasma cholesterol concentrations were determined weekly, and each point represents the mean±SEM. n=10 per group; \*\*\*P<0.001; G-control vs G-(P)RR. B, C, Pooled plasma samples were collected after the (B) first week of diet, or (C) after 4 weeks of diet, and the lipoprotein distribution was determined. The cholesterol content in each fraction was determined and is plotted. D, Two weeks after start of HFD diet, mice (n=6 per group) were injected with 50 µg Dil-labeled human LDL, and LDL clearance was assessed. Each point represents the mean±SEM, and the area under curve (AUC) was constructed for each treatment and used to compare the differences in LDL (low-density lipoprotein) clearance. \*P<0.05. E, Two weeks after (P)RR inhibition, mice were fasted for 6 hours, and VLDL (very-low-density lipoprotein) secretion was assessed (n=6 per group) by injecting mice with Pluronic F127 to inhibit lipoprotein lipase. Blood samples were drawn retro-orbitally at the indicated time points, and the concentration of triglycerides was determined, and the AUC was calculated and used to compare the differences in the rate of VLDL secretion. \*\*P<0.01; G-control vs G-(P)RR. F, G, Plasma triglyceride levels were analyzed in samples collected after 4 weeks of HFD. Each bar represents the mean±SEM, n=10 per group. \*\*\*P<0.001, or (G) pooled plasma samples were analyzed by FPLC (fast protein liquid chromatography). H, Plasma LPL (lipoprotein lipase) activity was determined for mice were injected with G-control or G-(P)RR and fed HFD for 4 weeks. n=9 per group. HDL indicates high-density lipoprotein; IDL, intermediate-density lipoprotein; and N.S., not significant.

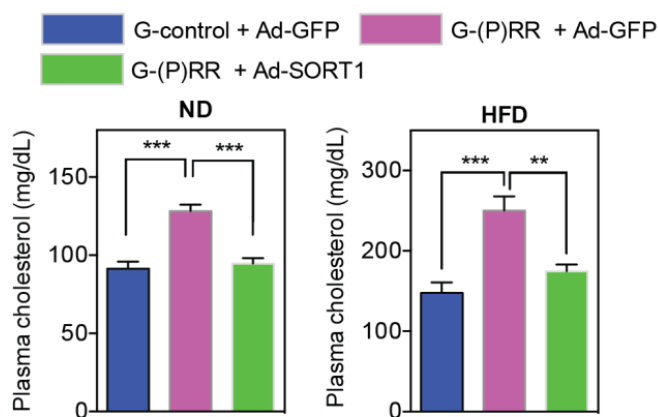
Because SORT1 deficiency *in vivo* reduces VLDL secretions and plasma triglycerides and (P)RR silencing decreases SORT1<sup>20,22,31</sup>, we wondered if the effect of (P)RR inhibition on hepatic lipid output is SORT1 dependent. To address this possibility, we studied plasma lipid levels in (P) RR-silenced mice in which we overexpressed hSORT1 (human SORT1). Exogenous hSORT1 protein was detected in liver, and hSORT1 partially rescued the (P)RR inhibition–induced LDLR protein reduction (Online Figure II). Given that SORT1 itself is a clearance receptor for LDL<sup>20–22</sup>, it is not surprising that hSORT1 overexpression reversed the (P) RR inhibition–induced increase in plasma cholesterol levels, primarily by decreasing the cholesterol content in the VLDL and IDL/LDL fractions (Figure 3A and 3B). However, hSORT1 overexpression did not prevent the reduction in plasma triglycerides caused by (P)RR inhibition (Figure 3C), implying that (P)RR inhibition reduced plasma triglycerides in a SORT1-independent manner.

### **Hepatic (P)RR Inhibition Reduced Plasma Cholesterol Levels in LDLR-Deficient Mice**

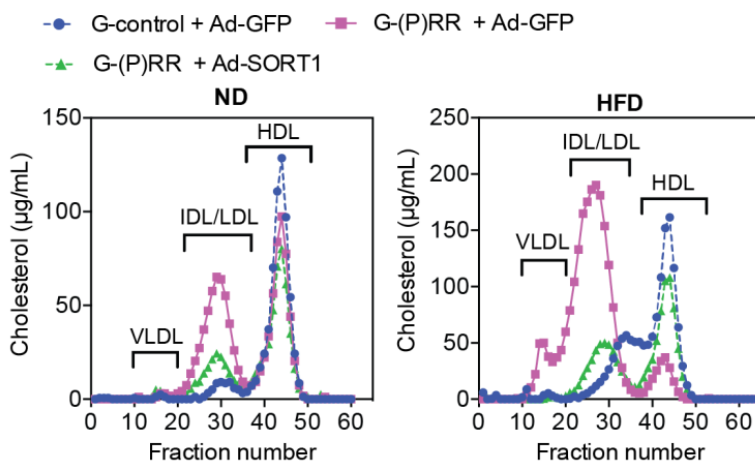
As (P)RR affects both hepatic LDL clearance and VLDL secretion, it is possible that (P)RR has a differential role in governing plasma cholesterol levels under distinct diet conditions. Under ND, LDL clearance may govern plasma cholesterol levels, whereas under HFD, VLDL secretion may become more prominent in determining plasma cholesterol levels. To address this issue, we tested the effects of hepatic (P)RR inhibition on plasma cholesterol levels in mice with impaired LDL clearance by

injecting adeno-associated virus expressing the gain-of-function PCSK9 (proprotein convertase subtilisin/kexin type 9) D377Y mutant<sup>32,33</sup> and in LDLR<sup>-/-</sup> mice. As expected, injecting C57BL/6 mice with the PCSK9 D377Y-encoding adeno-associated virus led to a marked increase in the circulating levels of LDL-C (from 76.74±1.72 to 167.3±2.27 mg/dL, n=39). We subsequently injected these mice with either saline, G-control, or G-(P)RR for 4 weeks and fed either ND or HFD. We found that after this treatment period, (P)RR inhibition reduced plasma cholesterol levels in both ND- and HFD-fed mice, despite the lack of functional LDLR-mediated clearance (Figure 4A through 4D). Similarly, inhibiting hepatic (P)RR in LDLR<sup>-/-</sup> mice induced a sustained decrease in plasma cholesterol levels independent of diet (Online Figure IIIA and IIIB).

**A**



**B**



**C**

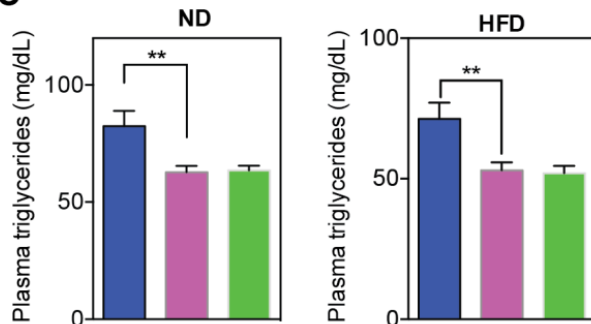


**Figure 3.** SORT1 (sortilin-1) overexpression prevents PRR-dependent hypercholesterolemia, but does not affect reduction in plasma triglycerides. Eight-week-old male C57BL/6 mice were injected with G-control or G-(pro)renin receptor (P)RR intraperitoneally and subsequently injected with either adenovirus carrying GFP (green fluorescent protein; Ad-GFP) or adenovirus carrying human SORT1 (Ad-SORT1) via the tail vein. Mice were fed with normal diet (ND) or high-fat diet (HFD) for 1 week and (A) plasma cholesterol levels were determined. Each bar represents the mean±SEM (n=6 per group). \*\*P<0.01; \*\*\*P<0.001. Alternatively, (B) lipoprotein composition in pooled plasma samples was analyzed by fractionation. C, Plasma was collected as in (A) and analyzed for triglyceride content. Each bar and error represent the mean±SEM (n=6 per group). \*\*P<0.01. HDL indicates high-density lipoprotein; IDL, intermediate-density lipoprotein; LDL, low-density lipoprotein; and VLDL, very-low-density lipoprotein.

These results confirm that LDL clearance is more dominant than VLDL secretion in determining circulating LDL levels in mice fed ND. Similar to the observation in wild-

type C57BL/6 mice, plasma triglycerides and VLDL-associated triglycerides were reduced by (P)RR inhibition under ND or HFD feeding (Figure 4E through 4H), in PCSK9-induced LDLR-deficient mice. Moreover, in LDLR<sup>-/-</sup> mice, hypertriglyceridemia was prevented by hepatic (P)RR inhibition (Online Figure IIIC and IIID). We reasoned that if (P)RR inhibition primarily affects lipid export pathways, we should observe lipid accumulation in liver, especially under HFD feeding. However, we found that hepatic lipid levels were also reduced by (P)RR inhibition (Figure 4I through 4K; Online Figure IV), implying that the reduced plasma lipid levels are not the result of impaired lipid secretion.

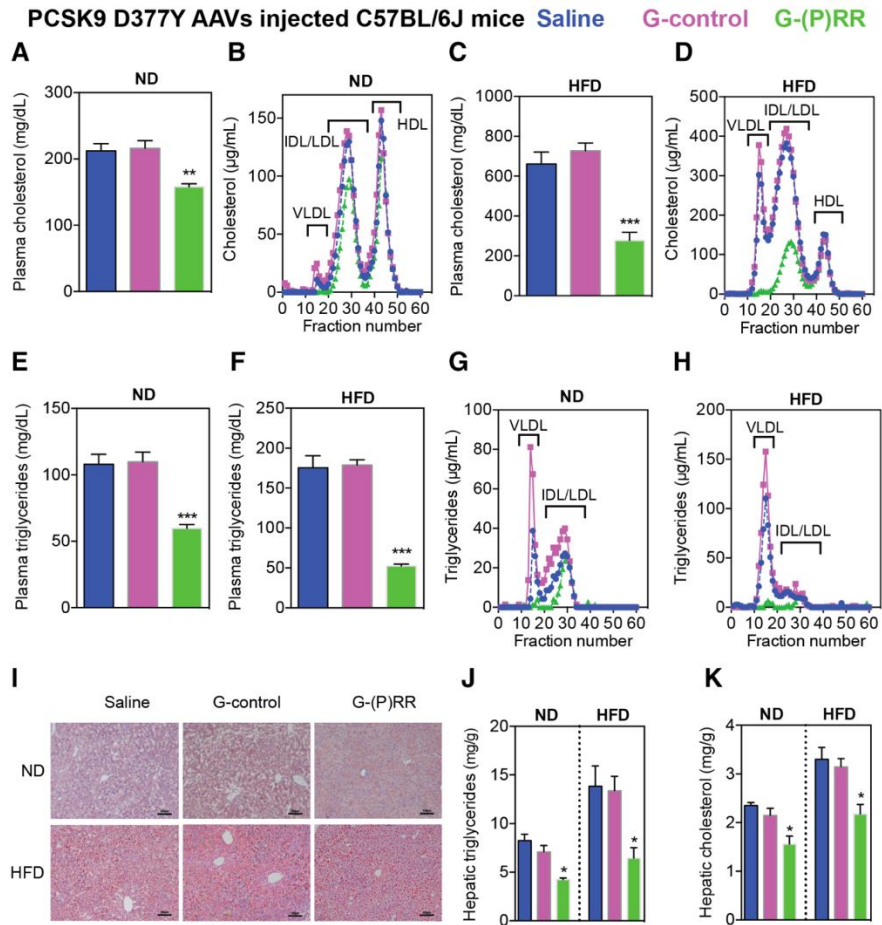


**Figure 4.** Hepatic (pro)renin receptor ([P]RR) inhibition in the absence of LDLR (low-density lipoprotein receptor) reduces plasma lipid levels and hepatic lipid deposition. Eight-week-old male C57BL/6 mice were injected intraperitoneally with  $10 \times 10^{10}$  genomic copies of mouse PCSK9 (proprotein convertase subtilisin/kexin type 9) D377Y adeno-associated virus (AAV), and fed with normal diet (ND) for 4 weeks. Subsequently, mice were injected with either saline (blue), G-control (magenta), or G-(P)RR (green) and fed with ND or high-fat diet (HFD) for an additional 4 weeks. A–D, Plasma cholesterol levels and lipoprotein profiles at the end of study were determined for ND-fed (A, B) and HFD-fed (C, D) mice. E–H, Plasma triglycerides and lipoprotein distribution were determined for ND-fed (E, G) and HFD-fed (F, H) mice. ( $n=6$  per group.) \*\* $P < 0.01$ ; \*\*\* $P < 0.001$ ; G-control vs G-(P)RR. I, Representative images of Oil Red O–stained liver samples from above-indicated mice fed with ND or HFD for 4 weeks. Scale bar=100  $\mu\text{m}$ . J, K, Lipids were extracted from liver samples and analyzed for triglycerides and cholesterol levels. \* $P < 0.05$ ; G-control vs G-(P)RR. HDL indicates high-density lipoprotein; IDL, intermediate-density lipoprotein; LDL, low-density lipoprotein; and VLDL, very-low-density lipoprotein.

### Hepatic (P)RR Inhibition Attenuated Diet-Induced Obesity and Improved Metabolic Disorders

(P)RR inhibition resulted in decreased hepatic VLDL secretion without concomitant hepatic lipid accumulation. This could point toward (P)RR regulating hepatic lipid biosynthesis, an important facet of fatty liver disease and obesity<sup>34</sup>. We therefore questioned whether hepatic (P)RR inhibition can ameliorate diet-induced fatty liver

disease and obesity. To address this, we inhibited hepatic (P)RR expression in C57BL/6 mice fed an HFD for 14 weeks. In line with our hypothesis, loss of hepatic (P)RR attenuated diet-induced obesity in C57BL/6 mice (Figure 5A). Body composition analyses using EchoMRI revealed that inhibiting hepatic (P)RR lowered fat weight of the mice, but did not affect the weight of lean mass (Figure 5B; Online Figure VA). Furthermore, the size of the livers and white adipose tissues of G-(P)RR-injected mice were smaller than control mice (Figure 5C and 5D). Under HFD, lipid accumulates in liver and increases liver weight. Mean liver weight of saline-injected or G-control-injected mice was  $\approx 2$  g, which was nearly twice the mean liver weight ( $1.07 \pm 0.02$  g;  $n=12$ ;  $P < 0.001$ ) of ND-fed C57BL/6 mice at same age (22 weeks old). Hepatic (P)RR inhibition attenuated HFD-induced liver weight gain and prevented abnormal lipid deposition in the liver (Figure 5E and 5F). Liver/body weight ratios of G-(P)RR-injected mice were also significantly lower than that of G-control-injected mice and resembled the ratio of ND-fed C57BL/6 mice at the same age (Online Figure VB). Moreover, mice in which hepatic (P)RR was inhibited had smaller adipocytes in inguinal white adipose tissues (Online Figure VC), but normal brown adipose tissues weight (Figure 5D). In agreement with reduced adipose tissues, plasma leptin concentrations were also reduced by hepatic (P)RR inhibition (Online Figure VD). However, plasma adiponectin concentrations were unaltered by (P)RR inhibition despite the marked reduction in adipose tissue weight (Online Figure VE), likely because of increased expression of adiponectin in white adipose tissues (Online Figure IC and IE). This suggests that hepatic (P)RR inhibition can indirectly affect adipokine secretion by adipose tissues, thereby contributing to improved metabolic control.

Accompanied by less body weight gain, fasting blood glucose concentrations were reduced by (P)RR inhibition (Online Figure VF), which also improved glucose tolerance and lowered plasma insulin levels (Online Figure VG and VH). Plasma AST (aspartate aminotransferase), ALT (alanine aminotransferase), and AST/ALT ratio indicate that (P)RR inhibition did not cause liver damage (Online Figure VI). In addition, H&E (hematoxylin and eosin) staining also revealed improved liver morphology by (P)RR inhibition (Figure 5E). Cumulative food intake of the mice during the 14-week experimental period was also recorded. G-(P)RR-injected mice consumed slightly less food than saline or G-control-injected mice, but when corrected for their body weight, their food consumption was actually higher (Online Figure VJ), suggesting that the reduced body weight gain is not because of reduced food intake. In addition, we did not observe any difference in blood pressure or heart rate among saline-injected, G-control-injected, or G-(P)RR-injected mice (Online Figure VK and VL), suggesting that the activity of the autonomic nervous system was not affected. We then monitored oxygen consumption and physical activity of the mice using metabolic cages. Inhibiting hepatic (P)RR increased oxygen consumption and 24-hour respiratory quotient of the mice, implying increased catabolism of energy sources (Figure 5G). Yet, physical activities of the mice were not different (Online

Figure VM). Collectively, these results support the beneficial metabolic effects of (P)RR inhibition.

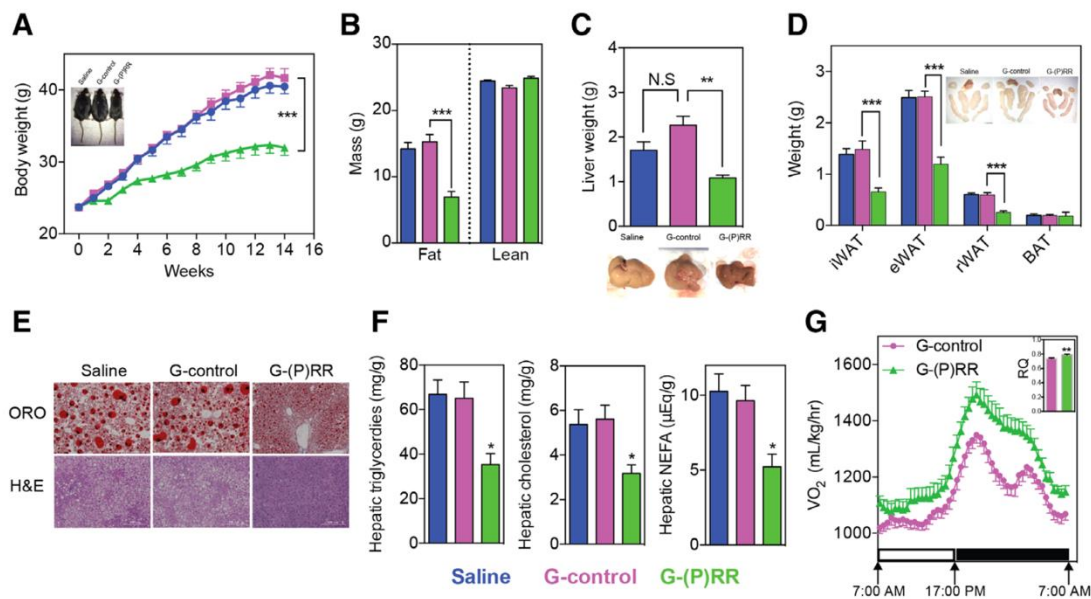


**Figure 5.** Hepatic (pro)renin receptor ((P)RR) inhibition attenuates diet-induced obesity and metabolic dysregulation. Eight-week-old mice were injected with saline (blue), G-control (magenta), or G-(P)RR (green) and fed a high-fat diet (HFD) for 14 weeks. (n=10 per group.) A, Body weight was monitored during the study period and each point and error represent the mean±SEM. \*\*\*P<0.001. Representative picture showing that G-(P)RR-injected mice are leaner than control mice. B, Fat and lean mass were measured by EchoMRI. Each bar and error represent the mean±SEM. \*\*\*P<0.001. C, Liver weight, and representative pictures showing G-(P)RR-treated mice have less fatty liver. \*\*P<0.01. D, Weight and representative picture of different adipose tissue depots. Brown fat tissue of saline and G-control-injected mice were surrounded with white fat which was removed to give a correct estimation of the weight of the brown fat. \*\*\*P<0.001. E, Representative images of Oil Red O (ORO) and H&E (hematoxylin and eosin) staining of the livers (scale bar=200 µm). F, Hepatic lipids were extracted and measured. \*P<0.05; G-control vs G-(P)RR. G, Oxygen consumption and 24-h average respiratory quotient (RQ) of G-control-injected and G-(P)RR-injected mice was monitored with a metabolic monitoring system 4 days before euthanize. n=8 per group. BAT indicates brown adipose tissue; eWAT, epididymal white adipose tissue; iWAT, inguinal white adipose tissue; N.S., not significant; and rWAT, retroperitoneal white adipose tissue.

### Inhibiting the (P)RR Upregulated Genes Involved in Fatty Acid Oxidation

Currently recognized functions of the (P)RR are not linked with lipid biosynthesis and energy homeostasis. To understand how (P)RR may regulate these processes, we transcriptionally profiled mice after (P)RR inhibition. Male mice (8 weeks old) were injected with either saline or G-(P)RR for 5 days, and liver samples were collected and extracted for total RNA and RNAseq analysis. We identified that (P)RR inhibition led to up- and downregulation of 199 genes and 202 genes, respectively (Online Table III). Gene ontology enrichment analysis revealed that metabolic pathways, including fatty acid (FA) degradation and elongation, were strongly

affected by (P)RR inhibition (Online Figure VIA and VIB). Among the affected genes, several genes involved in FA  $\beta$ -oxidation, such as *Hadha*, *Acaa2*, *Acadv1*, and *Acadl*, were upregulated by (P)RR inhibition, as confirmed by quantitative polymerase chain reaction (Online Figure VII). As such, increased FA  $\beta$ -oxidation may contribute to increased oxygen consumption and reduced hepatic lipid content.

### **Inhibiting (P)RR Reduced Protein Abundance of ACC and PDH**

To complement the RNA sequencing analysis and to better understand the function(s) of the (P)RR, we next performed comparative quantitative proteomics to identify hepatic proteins which are affected by (P)RR inhibition. Through this unbiased approach, we identified 191 and 116 proteins that were down- and upregulated, respectively, after (P)RR inhibition during feeding of either ND or HFD (Online Table IV). As reported previously, LDLR protein abundance was decreased by (P)RR inhibition (Online Table IV), validating the effectiveness of this approach to identify proteins with altered abundance. Gene ontology enrichment analyses revealed that proteins involved in lipid biosynthesis, lipid metabolism, and cholesterol metabolism were markedly affected by (P)RR inhibition (Online Figure VIC and VID). Among the identified proteins, PDH (pyruvate dehydrogenase), ACC $\alpha$  (acetyl-CoA carboxylase  $\alpha$ ), and ACC $\beta$  were markedly decreased. PDH is the enzyme responsible for converting pyruvate to acetyl-CoA and is a central metabolic node<sup>35</sup>. ACC catalyzes the formation of malonyl-CoA, an essential substrate for FA synthesis and a potent inhibitor of FA oxidation<sup>36</sup>. ACC is crucial in determining lipid storage and overall energy metabolism.<sup>37</sup> Thus, reduced PDH and ACC may contribute to increased FA oxidation and decreased lipid synthesis. To confirm this, we examined ACC $\alpha/\beta$  and PDH protein abundance in the liver of saline-injected, G-control-injected, or G-(P)RR-injected C57BL/6 mice fed with HFD for 14 weeks. Corroborating the proteomic-based approach, hepatic ACC $\alpha/\beta$ , PDHA (pyruvate dehydrogenase E1 component subunit  $\alpha$ ), and PDHB (pyruvate dehydrogenase E1 component subunit  $\beta$ ) were reduced by  $\approx$ 40% to 60% after hepatic (P)RR inhibition (Figure 6A), whereas the transcript abundance of ACC $\alpha/\beta$ , PDHA, and PDHB remained unaltered (Online Figure VII). Inhibiting the (P)RR in human hepatoma HepG2 cells with siRNAs also reduced protein abundances of ACC $\alpha/\beta$ , PDHA, and PDHB (Online Figure VIIIA), suggesting that this outcome is conserved in both mouse and humans. The (P)RR knockdown-induced reduction in ACC $\alpha/\beta$  protein abundance was partially reversed by the lysosome inhibitor bafilomycin A1, but was not affected by the autophagy inhibitor 3-methyladenine or the proteasome inhibitor MG-132 (Online Figure VIIIB), suggesting accelerated lysosome-dependent degradation of ACC $\alpha/\beta$  by (P)RR inhibition. In contrast, bafilomycin A1, 3-methyladenine, and MG-132 were unable to rescue (P)RR knockdown-induced reduction in PDHA and PDHB, implying that a different mechanism underlies the control of these proteins by (P)RR.

### **(P)RR Inhibition Reduced Cellular Acetyl-CoA Abundance and FA Synthesis in Hepatocytes**

Collectively, our results suggest that by reducing protein abundance of PDH, (P)RR inhibition reduces pyruvate to acetyl-CoA conversion and therefore reduces cellular acetyl-CoA production from glucose. Lower cellular acetyl-CoA levels will limit cellular FA and cholesterol synthesis. This biosynthetic block will be compounded by reduced ACC abundance, which will further limit FA synthesis. To test this hypothesis, we first measured relevant hepatic metabolites in mice injected with saline, G-control, or G-(P)RR and fed with HFD for 14 weeks. As expected, G-(P)RR-injected mice displayed hepatic pyruvate accumulation (Figure 6B), increased plasma pyruvate and lactate concentrations (Figure 6C and 6D), and decreased hepatic PDH activity (Figure 6E). Nevertheless, despite these changes, hepatic acetyl-CoA concentrations were unaltered by (P)RR inhibition (Figure 6F). Yet importantly, cellular acetyl-CoA levels in isolated mouse primary hepatocytes in which (P)RR was inhibited using G-(P)RR antisense oligonucleotide were reduced (Figure 6G). Similarly, acetyl-CoA levels were decreased by (P)RR inhibition in HepG2 cells, combined with a decrease in cellular PDH activity, increased cellular pyruvate concentrations and medium lactate concentrations, and reduced cellular lipid levels (Online Figure VIIC through VIIG). These data support our hypothesis and simultaneously suggest that *in vivo*, alternative sources, especially FAs supply, are available to overcome reduced pyruvate to acetyl-CoA conversion. This may also explain why acetyl-CoA levels were not reduced in the liver, as they were in HepG2 cells and primary hepatocytes. It is plausible that increased FA oxidation provides additional acetyl-CoA to compensate the increased energetic demand, which could also explain the increased oxygen consumption observed in G-(P)RR-injected mice. Therefore, we examined if (P)RR inhibition affects the oxygen consumption rate in mouse primary hepatocytes and HepG2 cells. As expected, inhibiting the (P)RR significantly increased basal oxygen consumption rate by  $\approx 50\%$  in mouse primary hepatocytes (Figure 6G) and  $\approx 30\%$  in HepG2 cells (Online Figure VIIC), and implying increased energy expenditure and utilization of high oxygen-consuming fuels such as FA. To fully understand the mechanism, we further examined cellular fuel dependency on long-chain FA in mouse primary hepatocytes and HepG2 cells. In the presence of  $50 \mu\text{mmol/L}$  oleic acid, long-chain FA accounted for  $\approx 20\%$  to  $30\%$  oxidized fuels (glucose, glutamine, and long-chain FA together) in control cells, whereas it accounted for  $>40\%$  oxidized fuels in primary mouse hepatocytes and HepG2 cells with (P)RR inhibited (Figure 6H; Online Figure VIIC). These data suggest that reduced acetyl-CoA supply from pyruvate is compensated by increased FA oxidation, as a mechanism to sustain cellular energy needs.

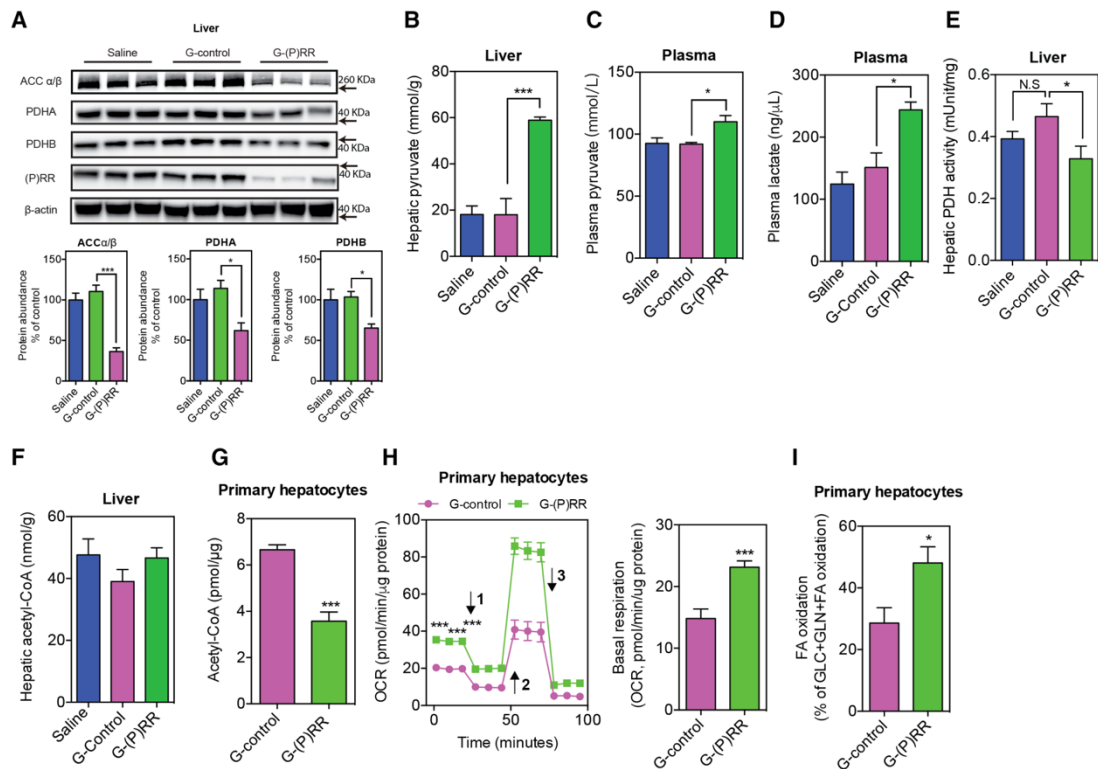


**Figure 6.** Inhibiting the (pro)renin receptor ([P]RR) reduces PDH (pyruvate dehydrogenase) and ACC (acetyl-CoA carboxylase) protein abundance and activity. A, Representative blot of liver samples from mice injected with saline, G-control, or G-(P)RR, and fed a high-fat diet (HFD) for 14 weeks. The protein abundance of PDHA (pyruvate dehydrogenase E1 component subunit  $\alpha$ ), PDHB (pyruvate dehydrogenase E1 component subunit  $\beta$ ), and ACC $\alpha/\beta$  was quantified and normalized to the level of  $\beta$ -actin in the same lysate. (n=6 per group); \*P<0.05; \*\*\*P<0.001. B, C57BL/6 mice were treated with antisense oligonucleotides (ASOs) and fed with HFD for 14 weeks. Hepatic pyruvate concentrations (B), plasma pyruvate concentrations (C), plasma lactate concentrations (D), hepatic PDH activity (E), and acetyl-CoA concentrations (F) were determined. G, Mouse primary hepatocytes were treated with G-control or G-(P)RR for 36 hours, and cellular Acetyl-CoA concentrations were determined. Three independent experiments in triplicates were performed. \*\*\*P<0.001. Oxygen consumption rate (OCR; H) and fuel dependency (I) were measured in mouse primary hepatocytes treated with G-control or G-(P)RR for 36 hours. Arrow 1 to 3 indicates addition of oligomycin, FCCP (carbonyl cyanide-4-[trifluoromethoxy] phenylhydrazone) and the mixture of rotenone and antimycin, respectively. n=6 per group. \*P<0.05; \*\*\*P<0.001. FA indicates fatty acid; and N.S., not significant.

## Discussion

We recently reported that the (P)RR is a novel modulator of LDL metabolism in vitro<sup>31</sup>. In the current study, we demonstrate that also in vivo, inhibiting the (P)RR in hepatocytes leads to defective LDL clearance as a result of reduced SORT1 and LDLR protein abundance. SORT1 is a recently identified hepatic clearance receptor for LDL, which also regulates VLDL secretion and plasma triglycerides<sup>16,20–22,38</sup>. SORT1 deficiency reduces VLDL secretion and plasma triglycerides<sup>20</sup> and in line with this, we found that (P)RR inhibition reduced VLDL secretion and plasma triglycerides, likely as a consequence of reduced SORT1. However, hepatic overexpression of hSORT1 in mice with (P)RR silencing was unable to prevent the

reduction in plasma triglycerides, despite completely preventing the increase in plasma LDL-C. This implies that the (P)RR regulates plasma triglycerides via a SORT1-independent manner. Furthermore, plasma LPL activity was not affected by (P)RR inhibition, excluding the possibility that increased triglyceride hydrolysis accounts for the reduced plasma triglycerides. In fact, hepatic lipid concentrations, including triglycerides and cholesterol, were both markedly reduced by (P)RR inhibition, indicating that lipid synthesis is diminished. Indeed, we found that the protein abundance of ACC, the crucial enzyme catalyzing the first step in FA synthesis, was markedly reduced by (P)RR inhibition. As a consequence, limited amounts of lipid being available for ApoB lipidation likely caused the reduction in plasma triglycerides. This may also explain why (P)RR inhibition even reduced plasma cholesterol levels in LDLR-deficient mice, in whom SORT1-dependent LDL clearance is impaired.

Our results raise the question of how the (P)RR regulates cellular lipid levels. Intriguingly, vacuolar H<sup>+</sup>-ATPase has recently been identified as a component of the mTORC1 (mechanistic target of rapamycin complex 1) pathway<sup>39</sup>. Indeed, acidification of lysosomes by vacuolar H<sup>+</sup>-ATPase is crucial for mTOR activation and function<sup>40</sup>. Increased mTORC1 activity is observed in genetic and HFD-induced obesity and has been implicated in the regulation of lipogenesis and VLDL secretion<sup>41-43</sup>. Knocking down the (P)RR reduces the protein levels of several subunits of the vacuolar H<sup>+</sup>-ATPase complex<sup>28-30,44</sup>. Consequently, (P)RR inhibition may prevent mTORC1 activation. Nevertheless, this seems unlikely as a recent report found that mTORC1 signaling was unaffected by (P)RR<sup>45</sup>.

An alternative explanation for the effect of (P)RR on hepatic lipid metabolism may be related to the renin-angiotensin system, which has been linked with obesity and lipid metabolism<sup>46</sup>. However, this too seems unlikely, as the affinity of (P)RR to (pro)renin is very low, and in fact, their interaction requires supraphysiological concentrations of (pro) renin. Rather, by using a combined unbiased transcriptome and proteomic approach, we now identified PDH and ACC as downstream effectors of (P)RR inhibition. (P)RR inhibition has previously been reported to reduce PDHB protein levels via a tyrosine-phosphorylation-dependent manner in mouse retina and human retinal pigment epithelium cells<sup>47</sup>. We found that both PDHA and PDHB were reduced by (P)RR inhibition. PDH is a ubiquitously expressed enzyme complex that catalyzes the conversion of pyruvate to acetyl-CoA<sup>48,49</sup>, acting as a central node that links lipid metabolism, glucose metabolism, and the tricarboxylic acid cycle. We thus speculated that by reducing PDH protein abundance and activity, (P)RR inhibition would reduce acetyl-CoA production from glucose and consequently diminish FA synthesis and increase FA oxidation (Figure 7)<sup>50</sup>. Indeed, this is what we observe in the livers of (P)RR-silenced mice. In addition, (P)RR inhibition also reduced ACC protein abundance. ACC plays an essential role in regulating FA synthesis and degradation<sup>37</sup>. Genetic deletion, or inhibition, of ACC reduces body weight gain and fat mass, suppresses triglycerides synthesis, and increases FA oxidation and energy

expenditure<sup>51,52</sup>, which resembles the phenotype of hepatic (P) RR inhibition. Moreover, PPAR $\gamma$  (peroxisome proliferator-activated receptor gamma) expression was reduced by (P) RR inhibition by  $\approx 50\%$  (Online Figure VII), and this may also have contributed to the reduced hepatic lipogenesis, as hepatic PPAR $\gamma$  plays important roles in HFD-induced up-regulation of lipogenic genes and de novo lipogenesis<sup>53-55</sup>. Recent studies have reported that genetically deleting adipose (P)RR in mice resulted in resistance to diet-induced obesity<sup>56</sup> and accelerated oxygen consumption<sup>57</sup>, yet causing severe hepatosteatosis.<sup>56</sup> Unaltered (P)RR expression in both white adipose tissues and brown adipose tissues excluded the possibility that adipose (P)RR deficiency also contributed to the observed phenotype in our study. However, it raises the question whether inhibiting the (P)RR in both adipose tissue and liver would provide additional beneficial effects in treating metabolic disorders.

Post-transcriptional regulation of ACC and PDH is not well understood, and thus, novel studies are required to fully understand their protein degradational regulation and the role of the (P)RR in this process. TRB3 (tribbles-related protein 3) has been reported to control ACC degradation under fasting conditions by coupling ACC to the E3 ligase COP1 (constitutive photomorphogenic protein 1)<sup>58</sup>. Interestingly, (P)RR inhibitions upregulated the expression of several E3 ligases, including HECTD1 (HECT domain E3 ubiquitin protein ligase 1; Online Table III), and both ACC $\alpha$  and ACC $\beta$  have been reported to interact with HECTD1<sup>59</sup>. It is therefore conceivable that (P)RR inhibition accelerates ACC degradation via lysosomes by upregulating HECTD1. Simultaneously, the (P)RR inhibition-induced reduction in PDH abundance is more difficult to understand. Inhibiting either autophagy, the lysosome or the proteasome, did not rescue this reduction, nor did inhibit mitophagy, a special form of autophagy involved in degradation of mitochondrial proteins (data not shown). This may suggest that (P)RR inhibition regulates PDH abundance via an as yet unsolved mechanism, as seems to be the case with SORT1 as well<sup>31</sup>.

In conclusion, we report that hepatic (P)RR is a crucial regulator of lipid metabolism. Inhibiting hepatic (P)RR reduced ACC and PDH protein levels and consequently increases FA oxidation and reduces lipid synthesis, thus attenuating diet-induced obesity and liver steatosis, as well as improving glycemic controls in C57BL/6 mice. Taken together, our study highlights the potential of inhibiting hepatic (P)RR as a therapeutic treatment for metabolic disorders such as fatty liver diseases and familial hypercholesterolemia.

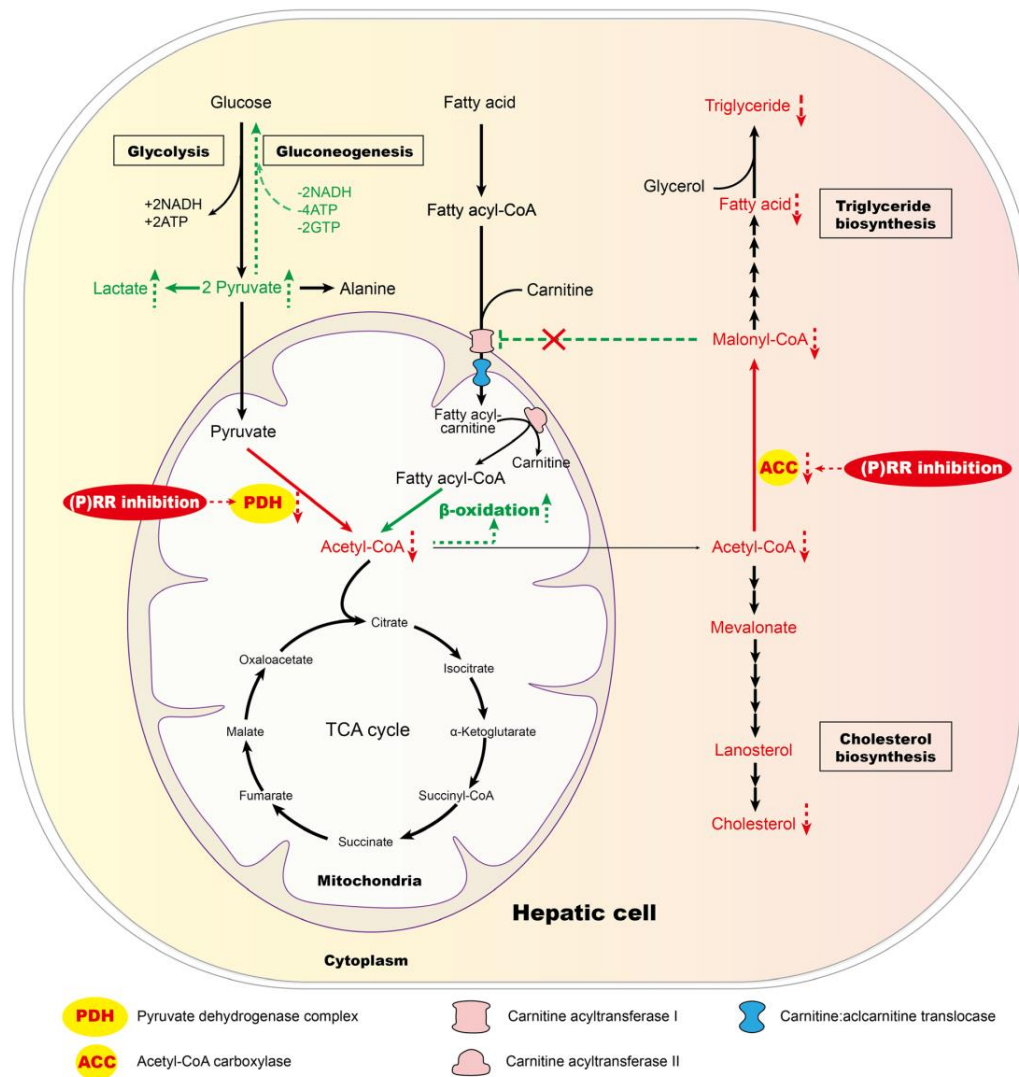


**Figure 7.** Model for reprogrammed hepatic metabolism by (pro)renin receptor ((P)RR) inhibition. Inhibiting hepatic (P)RR reduces PDH (pyruvate dehydrogenase) activity, impairing pyruvate metabolism and reducing acetyl-CoA supply from pyruvate, which limits fatty acid (FA) biosynthesis. (P)RR inhibition further limits FA biosynthesis by reducing protein abundance of ACC (acetyl-CoA carboxylase), the crucial enzyme in FA biosynthesis. It further signals to increase FA oxidation via reduced malonyl-CoA, an inhibitor of FA oxidation that blocks the transportation of long-chain fatty acylcarnitine by carnitine acyltransferase I (CAT1). TCA indicates tricarboxylic acid.

### Sources of Funding

X. Lu is supported by National Natural Science Foundation of China (grant no. 81500667), Shenzhen Municipal Science and Technology Innovation Council (grant no. JCYJ20160307160819191), and Shenzhen Peacock Plan (start-up fund). Y. Jiang is supported by National Natural Science Foundation of China (grant no. 81500354). X. Ruan is supported by Shenzhen Peacock Plan (grant no. KQTD20140630100746562), National Natural Science Foundation of China (Key Program, grant no. 81390354 and 81270789), and Shenzhen Municipal Science and Technology Innovation Council (grant no. JCYJ20140509172719310,

CXZZ20150601140615135). N. Zelcer is supported by a European Research Council Consolidator grant (617376) and is an Established Investigator of the Dutch Heart Foundation (2013T111). A.H.J. Danser is supported by the Top Institute Pharma (T2-301). F. Li is supported by National Natural Science Foundation of China (grant no. 81670702, 8170683), and the Natural Science Foundation of Guangdong (grant no. 2017030310646 and 2015A030313762), and the Science and Shenzhen Municipal Science and Technology Innovation Council (grant no. JCYJ20170307100154602).

## Disclosures

A.E. Mullick is an employee and shareholder of Ionis Pharmaceuticals. The other authors report no conflicts.

## References

1. Brown MS, Goldstein JL. A receptor-mediated pathway for cholesterol homeostasis. *Science*. 1986;232:34–47.
2. Spady DK. Hepatic clearance of plasma low density lipoproteins. *Semin Liver Dis*. 1992;12:373–385. doi: 10.1055/s-2008-1040407.
3. Olofsson SO, Stillemark-Billton P, Asp L. Intracellular assembly of VLDL: two major steps in separate cell compartments. *Trends Cardiovasc Med*. 2000;10:338–345.
4. Hooper AJ, van Bockxmeer FM, Burnett JR. Monogenic hypocholesterolemia lipid disorders and apolipoprotein B metabolism. *Crit Rev Clin Lab Sci*. 2005;42:515–545. doi: 10.1080/10408360500295113.
5. Innerarity TL, Mahley RW, Weisgraber KH, Bersot TP, Krauss RM, Vega GL, Grundy SM, Friedl W, Davignon J, McCarthy BJ. Familial defective apolipoprotein B-100: a mutation of apolipoprotein B that causes hyper-cholesterolemia. *J Lipid Res*. 1990;31:1337–1349.
6. Young SG, Hubl ST, Smith RS, Snyder SM, Terdiman JF. Familial hypo-beta lipoproteinemia caused by a mutation in the apolipoprotein B gene that results in a truncated species of apolipoprotein B (B-31). A unique mutation that helps to define the portion of the apolipoprotein B molecule required for the formation of buoyant, triglyceride-rich lipoproteins. *J Clin Invest*. 1990;85:933–942. doi: 10.1172/JCI114522.
7. Fan J, McCormick SP, Krauss RM, Taylor S, Quan R, Taylor JM, Young SG. Overexpression of human apolipoprotein B-100 in transgenic rabbits results in increased levels of LDL and decreased levels of HDL. *Arterioscler Thromb Vasc Biol*. 1995;15:1889–1899.
8. Bou Khalil M, Sundaram M, Zhang HY, Links PH, Raven JF, Manmontri B, Sariahmetoglu M, Tran K, Reue K, Brindley DN, Yao Z. The level and compartmentalization of phosphatidate phosphatase-1 (lipin-1) control the assembly and secretion of hepatic VLDL. *J Lipid Res*. 2009;50:47–58. doi: 10.1194/jlr.M800204-JLR200.
9. Yamazaki T, Sasaki E, Kakinuma C, Yano T, Miura S, Ezaki O. Increased very low density lipoprotein secretion and gonadal fat mass in mice over-expressing liver DGAT1. *J Biol Chem*. 2005;280:21506–21514. doi: 10.1074/jbc.M412989200.
10. Sharp D, Blinderman L, Combs KA, Kienzle B, Ricci B, Wager-Smith K, Gil CM, Turck CW, Bouma ME, Rader DJ. Cloning and gene defects in microsomal triglyceride transfer

protein associated with abetalipoproteinemia. *Nature*. 1993;365:65–69. doi: 10.1038/365065a0.

11. Hobbs HH, Brown MS, Goldstein JL. Molecular genetics of the LDL receptor gene in familial hypercholesterolemia. *Hum Mutat*. 1992;1:445–466. doi: 10.1002/humu.1380010602.

12. Khachadurian AK, Uthman SM. Experiences with the homozygous cases of familial hypercholesterolemia. A report of 52 patients. *Nutr Metab*. 1973;15:132–140.

13. Soutar AK, Naoumova RP. Mechanisms of disease: genetic causes of familial hypercholesterolemia. *Nat Clin Pract Cardiovasc Med*. 2007;4:214–225. doi: 10.1038/ncpcardio0836.

14. Kathiresan S, Willer CJ, Peloso GM, et al. Common variants at 30 loci contribute to polygenic dyslipidemia. *Nat Genet*. 2009;41:56–65. doi: 10.1038/ng.291.

15. Kathiresan S, Melander O, Guiducci C, et al. Six new loci associated with blood low-density lipoprotein cholesterol, high-density lipoprotein cholesterol or triglycerides in humans. *Nat Genet*. 2008;40:189–197. doi: 10.1038/ng.75.

16. Linsel-Nitschke P, Heeren J, Aherrahrou Z, et al. Genetic variation at chromosome 1p13.3 affects sortilin mRNA expression, cellular LDL-uptake and serum LDL levels which translates to the risk of coronary artery disease. *Atherosclerosis*. 2010;208:183–189. doi: 10.1016/j.atherosclerosis.2009.06.034.

17. Muendlein A, Geller-Rhomberg S, Saely CH, Winder T, Sonderegger G, Rein P, Beer S, Vonbank A, Drexel H. Significant impact of chromosomal locus 1p13.3 on serum LDL cholesterol and on angiographically characterized coronary atherosclerosis. *Atherosclerosis*. 2009;206:494–499. doi: 10.1016/j.atherosclerosis.2009.02.040.

18. Sandhu MS, Waterworth DM, Debenham SL, et al; Wellcome Trust Case Control Consortium. LDL-cholesterol concentrations: a genome-wide association study. *Lancet*. 2008;371:483–491. doi: 10.1016/S0140-6736(08)60208-1.

19. Willer CJ, Sanna S, Jackson AU, et al. Newly identified loci that influence lipid concentrations and risk of coronary artery disease. *Nat Genet*. 2008;40:161–169. doi: 10.1038/ng.76.

20. Kjolby M, Andersen OM, Breiderhoff T, Fjorback AW, Pedersen KM, Madsen P, Jansen P, Heeren J, Willnow TE, Nykjaer A. Sort1, encoded by the cardiovascular risk locus 1p13.3, is a regulator of hepatic lipoprotein export. *Cell Metab*. 2010;12:213–223. doi: 10.1016/j.cmet.2010.08.006.

21. Musunuru K, Strong A, Frank-Kamenetsky M, et al. From noncoding variant to phenotype via SORT1 at the 1p13 cholesterol locus. *Nature*. 2010;466:714–719. doi: 10.1038/nature09266.

22. Strong A, Ding Q, Edmondson AC, et al. Hepatic sortilin regulates both apolipoprotein B secretion and LDL catabolism. *J Clin Invest*. 2012;122:2807–2816. doi: 10.1172/JCI63563.

23. Tveten K, Strøm TB, Cameron J, Berge KE, Leren TP. Mutations in the SORT1 gene are unlikely to cause autosomal dominant hypercholesterolemia. *Atherosclerosis*. 2012;225:370–375. doi: 10.1016/j.atherosclerosis.2012.10.026.

24. Batenburg WW, Lu X, Leijten F, Maschke U, Müller DN, Danser AH. Renin- and prorenin-induced effects in rat vascular smooth muscle cells overexpressing the human

(pro)renin receptor: does (pro)renin-(pro)renin receptor interaction actually occur? Hypertension. 2011;58:1111–1119. doi:10.1161/HYPERTENSIONAHA.111.180737.

25. Batenburg WW, Danser AH. (Pro)renin and its receptors: pathophysiological implications. Clin Sci (Lond). 2012;123:121–133. doi: 10.1042/CS20120042.
26. Cruciat CM, Ohkawara B, Acebron SP, Karaulanov E, Reinhard C, Ingelfinger D, Boutros M, Niehrs C. Requirement of prorenin receptor and vacuolar H<sup>+</sup>-ATPase-mediated acidification for Wnt signaling. Science. 2010;327:459–463. doi: 10.1126/science.1179802.
27. Geisberger S, Maschke U, Gebhardt M, Kleinewietfeld M, Manzel A, Linker RA, Chidgey A, Dechend R, Nguyen G, Daumke O, Muller DN, Wright MD, Binger KJ. New role for the (pro)renin receptor in T-cell development. Blood. 2015;126:504–507. doi: 10.1182/blood-2015-03-635292.
28. Kinouchi K, Ichihara A, Sano M, Sun-Wada GH, Wada Y, Kurauchi-Mito A, Bokuda K, Narita T, Oshima Y, Sakoda M, Tamai Y, Sato H, Fukuda K, Itoh H. The (pro)renin receptor/ATP6AP2 is essential for vacuolar H<sup>+</sup>-ATPase assembly in murine cardiomyocytes. Circ Res. 2010;107:30–34. doi: 10.1161/CIRCRESAHA.110.224667.
29. Oshima Y, Kinouchi K, Ichihara A, Sakoda M, Kurauchi-Mito A, Bokuda K, Narita T, Kurosawa H, Sun-Wada GH, Wada Y, Yamada T, Takemoto M, Saleem MA, Quaggin SE, Itoh H. Prorenin receptor is essential for normal podocyte structure and function. J Am Soc Nephrol. 2011;22:2203–2212. doi: 10.1681/ASN.2011020202.
30. Riediger F, Quack I, Qadri F, et al. Prorenin receptor is essential for podocyte autophagy and survival. J Am Soc Nephrol. 2011;22:2193–2202. doi: 10.1681/ASN.2011020200.
31. Lu X, Meima ME, Nelson JK, Sorrentino V, Loregger A, Scheij S, Dekkers DH, Mulder MT, Demmers JA, M-Dallinga-Thie G, Zelcer N, Danser AH. Identification of the (pro)renin receptor as a novel regulator of low-density lipoprotein metabolism. Circ Res. 2016;118:222–229. doi: 10.1161/CIRCRESAHA.115.306799.
32. Lu H, Howatt DA, Balakrishnan A, Graham MJ, Mullick AE, Daugherty A. Hypercholesterolemia induced by a PCSK9 gain-of-function mutation augments angiotensin II-induced abdominal aortic aneurysms in C57BL/6 mice—brief report. Arterioscler Thromb Vasc Biol. 2016;36:1753–1757. doi: 10.1161/ATVBAHA.116.307613.
33. Goettsch C, Hutcheson JD, Hagita S, Rogers MA, Creager MD, Pham T, Choi J, Mlynarchik AK, Pieper B, Kjolby M, Aikawa M, Aikawa E. A single injection of gain-of-function mutant PCSK9 adeno-associated virus vector induces cardiovascular calcification in mice with no genetic modification. Atherosclerosis. 2016;251:109–118. doi: 10.1016/j.atherosclerosis.2016.06.011.
34. Postic C, Girard J. Contribution of de novo fatty acid synthesis to hepatic steatosis and insulin resistance: lessons from genetically engineered mice. J Clin Invest. 2008;118:829–838. doi: 10.1172/JCI34275.
35. Sugden MC, Holness MJ. Recent advances in mechanisms regulating glucose oxidation at the level of the pyruvate dehydrogenase complex by PDKs. Am J Physiol Endocrinol Metab. 2003;284:E855–E862. doi: 10.1152/ajpendo.00526.2002.
36. Foster DW. Malonyl-CoA: the regulator of fatty acid synthesis and oxidation. J Clin Invest. 2012;122:1958–1959.
37. Tong L. Acetyl-coenzyme A carboxylase: crucial metabolic enzyme and attractive target for drug discovery. Cell Mol Life Sci. 2005;62:1784–1803. doi: 10.1007/s00018-005-5121-4.

38. Teslovich TM, Musunuru K, Smith AV, et al. Biological, clinical and population relevance of 95 loci for blood lipids. *Nature*. 2010;466:707–713. doi: 10.1038/nature09270.
39. Zoncu R, Bar-Peled L, Efeyan A, Wang S, Sancak Y, Sabatini DM. mTORC1 senses lysosomal amino acids through an inside-out mechanism that requires the vacuolar H(+)-ATPase. *Science*. 2011;334:678–683. doi: 10.1126/science.1207056.
40. Hu Y, Carraro-Lacroix LR, Wang A, Owen C, Bajenova E, Corey PN, Brumell JH, Voronov I. Lysosomal pH plays a key role in regulation of mTOR activity in osteoclasts. *J Cell Biochem*. 2016;117:413–425. doi: 10.1002/jcb.25287.
41. Li S, Brown MS, Goldstein JL. Bifurcation of insulin signaling pathway in rat liver: mTORC1 required for stimulation of lipogenesis, but not inhibition of gluconeogenesis. *Proc Natl Acad Sci USA*. 2010;107:3441–3446. doi: 10.1073/pnas.0914798107.
42. Peterson TR, Sengupta SS, Harris TE, Carmack AE, Kang SA, Balderas E, Guertin DA, Madden KL, Carpenter AE, Finck BN, Sabatini DM. mTOR complex 1 regulates lipin 1 localization to control the SREBP pathway. *Cell*. 2011;146:408–420. doi: 10.1016/j.cell.2011.06.034.
43. Ai D, Baez JM, Jiang H, Conlon DM, Hernandez-Ono A, Frank-Kamenetsky M, Milstein S, Fitzgerald K, Murphy AJ, Woo CW, Strong A, Ginsberg HN, Tabas I, Rader DJ, Tall AR. Activation of ER stress and mTORC1 suppresses hepatic sortilin-1 levels in obese mice. *J Clin Invest*. 2012;122:1677–1687. doi: 10.1172/JCI61248.
44. Lu X, Garrelds IM, Wagner CA, Danser AH, Meima ME. (Pro)renin receptor is required for prorenin-dependent and -independent regulation of vacuolar H<sup>+</sup>-ATPase activity in MDCK.C11 collecting duct cells. *Am J Physiol Renal Physiol*. 2013;305:F417–F425. doi: 10.1152/ajprenal.00037.2013.
45. Kissing S, Rudnik S, Damme M, Lüllmann-Rauch R, Ichihara A, Kornak U, Eskelinen EL, Jabs S, Heeren J, De Brabander JK, Haas A, Saftig P. Disruption of the vacuolar-type H<sup>+</sup>-ATPase complex in liver causes MTORC1-independent accumulation of autophagic vacuoles and lysosomes. *Autophagy*. 2017;13:670–685. doi:10.1080/15548627.2017.1280216.
46. Engeli S, Negrel R, Sharma AM. Physiology and pathophysiology of the adipose tissue renin-angiotensin system. *Hypertension*. 2000;35:1270–1277.
47. Kanda A, Noda K, Ishida S. ATP6AP2/(pro)renin receptor contributes to glucose metabolism via stabilizing the pyruvate dehydrogenase E1  $\beta$  sub-unit. *J Biol Chem*. 2015;290:9690–9700. doi: 10.1074/jbc.M114.626713.
48. Patel MS, Nemeria NS, Furey W, Jordan F. The pyruvate dehydrogenase complexes: structure-based function and regulation. *J Biol Chem*. 2014;289:16615–16623. doi: 10.1074/jbc.R114.563148.
49. Harris RA, Bowker-Kinley MM, Huang B, Wu P. Regulation of the activity of the pyruvate dehydrogenase complex. *Adv Enzyme Regul*. 2002;42:249–259.
50. Sun Y, Danser AHJ, Lu X. (Pro)renin receptor as a therapeutic target for the treatment of cardiovascular diseases? *Pharmacol Res*. 2017;125(pt A):48–56.
51. Choi CS, Savage DB, Abu-Elheiga L, Liu ZX, Kim S, Kulkarni A, Distefano A, Hwang YJ, Reznick RM, Codella R, Zhang D, Cline GW, Wakil SJ, Shulman GI. Continuous fat oxidation in acetyl-CoA carboxylase 2 knockout mice increases total energy expenditure,

reduces fat mass, and improves insulin sensitivity. *Proc Natl Acad Sci USA*. 2007;104:16480–16485. doi: 10.1073/pnas.0706794104.

52. Abu-Elheiga L, Matzuk MM, Abo-Hashema KA, Wakil SJ. Continuous fatty acid oxidation and reduced fat storage in mice lacking acetyl-CoA carboxylase 2. *Science*. 2001;291:2613–2616. doi: 10.1126/science.1056843.

53. Inoue M, Ohtake T, Motomura W, Takahashi N, Hosoki Y, Miyoshi S, Suzuki Y, Saito H, Kohgo Y, Okumura T. Increased expression of PPAR $\gamma$  in high fat diet-induced liver steatosis in mice. *Biochem Biophys Res Commun*. 2005;336:215–222. doi: 10.1016/j.bbrc.2005.08.070.

54. Gavrilova O, Haluzik M, Matsusue K, Cutson JJ, Johnson L, Dietz KR, Nicol CJ, Vinson C, Gonzalez FJ, Reitman ML. Liver peroxisome proliferator-activated receptor  $\gamma$  contributes to hepatic steatosis, triglyceride clearance, and regulation of body fat mass. *J Biol Chem*. 2003;278:34268–34276. doi: 10.1074/jbc.M300043200.

55. Zhang YL, Hernandez-Ono A, Siri P, Weisberg S, Conlon D, Graham MJ, Croke RM, Huang LS, Ginsberg HN. Aberrant hepatic expression of PPAR $\gamma$ 2 stimulates hepatic lipogenesis in a mouse model of obesity, insulin resistance, dyslipidemia, and hepatic steatosis. *J Biol Chem*. 2006;281:37603–37615. doi: 10.1074/jbc.M604709200.

56. Wu CH, Mohammadmoradi S, Thompson J, Su W, Gong M, Nguyen G, Yiannikouris F. Adipocyte (pro)renin-receptor deficiency induces lipodystrophy, liver steatosis and increases blood pressure in male mice. *Hypertension*. 2016;68:213–219. doi: 10.1161/HYPERTENSIONAHA.115.06954.

57. Shamansurova Z, Tan P, Ahmed B, Pepin E, Seda O, Lavoie JL. Adipose tissue (P)RR regulates insulin sensitivity, fat mass and body weight. *Mol Metab*. 2016;5:959–969. doi: 10.1016/j.molmet.2016.08.009.

58. Qi L, Heredia JE, Altarejos JY, Sreaton R, Goebel N, Niessen S, Macleod IX, Liew CW, Kulkarni RN, Bain J, Newgard C, Nelson M, Evans RM, Yates J, Montminy M. TRB3 links the E3 ubiquitin ligase COP1 to lipid metabolism. *Science*. 2006;312:1763–1766. doi: 10.1126/science.1123374.

59. Rouillard AD, Gunderson GW, Fernandez NF, Wang Z, Monteiro CD, McDermott MG, Ma'ayan A. The harmonizome: a collection of processed datasets gathered to serve and mine knowledge about genes and proteins. *Database (Oxford)*. 2016;2016:baw100.

## **Supplemental Materials**

### **Methods:**

#### **Animals**

C57BL/6 mice and LDLR<sup>-/-</sup> mice were obtained from Model Animal Research Center of Nanjing University (Nanjing, China), and were housed at a 10-hour light/14-hour dark cycle. 8-week old male C57BL/6 mice were injected weekly with saline, GalNAc control ASOs (G-control), or GalNAc (P)RR ASOs [G-(P)RR] subcutaneously. For experiments  $\leq$  4 weeks, ASOs were dosed at 3 mg/kg/week. For experiments  $\geq$  4 weeks, ASOs were dosed at 3 mg/kg/week in the first 4 weeks, and were then reduced to 1.5 mg/kg/week until end of the experiment. Mice were either fed with ND (Harlan Teklad) or HFD (42% kcal fat, 0.2% cholesterol, Harlan Teklad). LDLR<sup>-/-</sup> mice were treated in the same way as C57BL/6 mice. Body weight was monitored weekly. Food consumption of each cage hosting 6 mice was recorded weekly. Blood samples were collected via submandibular bleeding after 6h fasting. Plasma lipid TC and TG levels were monitored bi-weekly, unless indicated elsewhere. Experimental procedures were approved by local animal ethics committee (no. 2014-0140).

#### **Antisense Oligonucleotides (ASOs)**

ASOs with 5'-methyl modified cytosine and a phosphorothioate backbone containing 2-O, 4-C-[(S)-ethylidene]- D-ribose (cEt) modified sugars were synthesized as described previously<sup>1</sup>. Chimeric ASOs containing 16mer cEt chemistries were used with the gapmer design of 3-10-3 wherein the terminal 5' and 3' nucleotides contained the cET modified sugars that flanked 10 nucleotides with unmodified sugars. The liver targeting conjugate GalNAc was connected through a tris-hexylamino-(THA)-C6 linker at the 5' end of the ASO<sup>2</sup>. Extensive in vitro activity screens were performed followed by in vivo tolerability and activity studies to identify the lead (P)RR ASO with the following nucleotide sequence AGATATTGGTCCATTT. A control ASO that did not hybridize to any known rodent mRNA was used and had the following nucleotide sequence, GGCCAATACGCCGTCA.

#### **Intraperitoneal glucose tolerance test (IPGTT)**

IPGTT was performed as described elsewhere<sup>3</sup>, one week prior to the end of the study. Briefly, following 16h fasting, 2 g/kg glucose was injected intraperitoneally to mice. Blood samples were collected from tail vein at 0, 15, 30, 60 and 120 min after glucose injection, and blood glucose was measured using a glucometer (Roche). Glucose levels at each time point were compared, and overall differences in glycemic control were compared using area under curve (AUC).

#### **In vivo LDL clearance assay**

In vivo LDL clearance was measured as described before<sup>4</sup>. In short, mice were injected with 50  $\mu$ g human Dil-labeled LDL (AngYuBio, Shanghai) via a tail-vein.

Then, blood samples were collected retro-orbitally at 2, 10, 20, 40, 80, 160, and 300 min after injection. A standard curve was constructed by serial dilution of the human Dil-labeled LDL into mice plasma. Dil-LDL concentrations at 2 min after injection were the highest and were thus set as the baseline value for further analysis. Differences in VLDL secretion were compared using area under curve (AUC).

### **Hepatic VLDL secretion**

To determine VLDL-TG secretion rate, mice were fasted for 4 hours and injected intraperitoneally with 1 mg/g Pluronic F127 (Sigma Aldrich), a detergent that inhibits lipolysis. Subsequently, blood samples were collected by retroorbital bleeding at 0, 1, 2 and 4 hours after Pluronic F127 injection. Differences in VLDL secretion were compared using area under curve (AUC).

### **Fast Protein Liquid Chromatography (FPLC) analysis of plasma lipoproteins**

FPLC analysis of plasma lipoproteins was performed as described before<sup>5</sup>. In short, plasma samples were pooled, and cleared by centrifugation and filtering through a 0.22  $\mu$ m filter. 200  $\mu$ L cleared plasma samples were loaded for FPLC analysis using an AKTA purifier (GE) and Superose-6 Increase 10/300 GL (GE). Flow rate was set to 0.5 mL/min, and fractions between 10-16 mL were collected at intervals of 0.25 mL/fraction. Cholesterol and triglycerides content in each fraction was measured.

### **Oxygen consumption and physical activity measurement**

Metabolic and physical activity of the mice were measured using an indirect open-circuit calorimeter (Oxylet, Panlab) <sup>6</sup>. Mice were housed individually in metabolic chambers and oxygen consumption, CO<sub>2</sub> production, and physical activity were recorded at 30 min intervals for consecutive 48 hours. For accuracy, the recorded data from the first 12-14 hours after the mice have been housed in the chamber were not analyzed.

### **Body composition analysis**

Fat and lean mass composition of the mice were evaluated by EchoMRI (Echo Medical Systems, Houston, TX, USA) before sacrifice. Weights of different fat tissues were measured using a scale balance with 0.0001-gram accuracy (Sartorius).

### **H&E staining and Oil Red O staining**

Hematoxylin and eosin (H&E) staining was performed on 5  $\mu$ m tissue sections which were Bouin's-fixed and paraffin-embedded. Oil Red O staining was used to detect hepatic neutral lipids. Fresh liver and adipose tissues embedded in OCT were cryosectioned for 7  $\mu$ m. After fixation with 4% paraformaldehyde, sections were stained with 0.3% oil red o following standard procedures<sup>7</sup> and then counterstained with hematoxylin. Images were scanned using Cytation 5 Cell Imaging Multi-mode reader (Biotek).

### **Measurement of ALT and AST**

Blood samples were precleared by centrifugation at 3,000×g for 5 minutes. Plasma alanine aminotransferase (ALT) and aspartate aminotransferase (AST) activities were measured by commercial kits (Biosino) following the manufacture's protocol.

### **Adenovirus and Adeno-associated virus**

Adeno-associated virus (AAV) expressing the D377Y PCSK9 mutant and their use was previously described<sup>8</sup>. Eight-week-old mice were intraperitoneally with AAV-PCSK9 at a concentration of 10×10<sup>10</sup> genomic copies, and fed a chow-diet for 4 weeks to induce LDLR degradation. Afterwards, mice were treated with saline, G-control, or G-(P)RR for 4 weeks, and fed with chow or HFD. Human SORT1 under control of a CMV promotor was cloned and inserted in to pAd-EF1a-GFP vector (Vigenebio, China). Packaging of adenovirus was performed by linearization of the plasmid and transfection of 293A cells. Adenoviral particles were purified by ultracentrifugation, and virus titer was determined by serial dilution and plaque formation. 8-weeks old male mice were injected with 1.5×10<sup>9</sup> pfu Ad-hSORT1 or Ad-GFP (purchased from Vigenebio) via tail-vein. Mice were fed with chow or HFD for 7 days, and sacrificed after 6h fasting.

### **Transcriptome analysis**

To assess whether silencing hepatic (P)RR affects gene expression in the liver, we injected mice (3 mice/group) intraperitoneally with saline or G -(P)RR as described above. After 5 days, the mice were sacrificed after 6h fasting, and liver samples were collected immediately and stored in Trizol at -80 °C until use. Total RNA was extracted and a RNA sequencing library was constructed for each sample using the Illumina Mrna-Seq Prep Kit. Paired-End libraries were prepared following Illumina's protocols and sequenced on the Illumina HiSeq X10 platform. RNA Sequencing reads were analyzed following the reported protocol with HISAT, StringTie and Ballgown<sup>9</sup>. More specifically, high quality sequencing reads were firstly mapped to the mouse reference genome (version Ensembl GRCm38) using HISAT with default parameters<sup>10</sup>. Transcriptomic expression at gene and transcript level, characterized by FPKM (Fragments Per Kilobase of transcript per Million mapped reads), was then quantified by StringTie<sup>9</sup>. The Ballgown package was used to identify differential expressed genes (DEGs) with P <0.05 between G-(P)RR and saline control<sup>11</sup>. Functional analysis of all DEGs was performed using DAVID functional annotation clustering tool<sup>12</sup>. Gene numbers were calculated for each Gene ontology (GO) category, and a hypergeometric test was used to identify significantly enriched GO categories in DEGs.

### **Comparative proteomics using iTRAQ**

To understand how does (P)RR inhibition affects lipid metabolism and energy metabolism, we performed comparative proteomics analysis. Mice (n=3/group) were treated with G-control or G-(P)RR for 4 weeks, and fed with chow or HFD. Mice were sacrificed after 6h fasting. Livers were collected and homogenized in lysis buffer by TissueLyzer. Proteins were precipitated by acetone and resuspended with

dissolving buffer containing 6 M guanidine hydrochloride and 300 mM TEAB (triethylammonium bicarbonate). Protein concentrations were determined by BCA, and equal amounts of proteins from individual samples per group were mixed and processed for iTRAQ labeling. Labeled samples were fractionated by high pH separation using Acquity UPLC H-Class Bio system (Waters Corporation, Milford, MA) connected to a reverse phase column (XBridge C18 column, 2.1 mm×150 mm, 3.5 μm, 300 Å, Waters Corporation, Milford, MA). High pH separation was performed using a linear gradient, starting from 5% B to 35% B in 40 min (B: 5 mM ammonium formate in 90% acetonitrile, pH 10.0, adjusted with ammonium hydroxide). The column flow rate was maintained at 200 μL/min and column temperature was maintained at room temperature. Ten fractions were collected. Each fraction was dried in a vacuum concentrator for the next step. The peptide samples were resuspended with 30 μL solvent A respectively (A: water with 0.1% formic acid; B: acetonitrile with 0.1% formic acid), separated by nano-RPLC (EASY -nLC 1000, Thermo Fisher Scientific) and analyzed by online electrospray tandem mass spectrometry (Q Exactive mass spectrometer, Thermo Fisher Scientific). 5 μL peptide sample was loaded onto the trap column (Thermo Scientific Acclaim PepMap C18, 75 μm × 2 cm), and subsequently separated on the analytical column (Acclaim PepMap C18, 75 μm × 15 cm) with a linear gradient, from 5% B to 35% B in 70 min, at a flow rate of 300 nL/min. The electrospray voltage of 1.6 kV versus the inlet of the mass spectrometer was used. The Q Exactive mass spectrometer was operated in the data-dependent mode to switch automatically between MS and MS/MS acquisition. Survey full -scan MS spectra (m/z 300 -1600) were acquired in Orbitrap with a mass resolution of 70,000 at m/z 200. The AGC target was set to 1 000 000, and the maximum injection time was 20 ms. The ten most intense peaks were isolated in the quadrupole with isolation window of 2.0 m/z units. Ions with charge states 2+, 3+, and 4+ were sequentially fragmented by higher energy collisional dissociation (HCD) with a normalized collision energy of 27%, fixed first mass was set at 100, and further analyzed in the Orbitrap mass analyzer with 17,500 resolution. The AGC target was set to 500,000, and the maximum injection time was 200 ms. In all cases, one microscan was recorded using dynamic exclusion of 35 seconds.

The expression ratio [G-(P)RR/G -control] was calculated for each protein, under different diet conditions. Cut -off value was set to 1.2-fold [G-(P)RR/G-control >1.2 or <0.083]. Proteins with altered abundance were compared between HFD and chow, and only proteins that were regulated in the same trend by (P)RR inhibition were identified as differential expressed proteins (DEPs). Functional analysis of all DEGs was preformed using DAVID functional annotation clustering tool. Gene numbers were calculated for each Gene ontology (GO) category, and hypergeometric test was used to identify significantly enriched GO categories in DEGs.

### **Measurement of pyruvate, acetyl-CoA, lactate and PDH activity**

Plasma pyruvate and lactate levels were detected using Pyruvate Assay kit (Sigma Aldrich) and Lactate Assay kit (Sigma Aldrich), following the manufacture's

protocols. To measure hepatic pyruvate, acetyl-CoA, and PDH activity, liver samples (~25 mg) were homogenized in the assay buffers provided with the kits, and measurements were performed according to the manufacturer's protocol. To measure cellular pyruvate levels, HepG2 cells were transfected with either control siRNA (siNC) or (P)RR siRNA [si(P)RR] for 48 hours. Cells were then detached using TrypLE and collected by centrifugation at 4 °C at 100x g, followed by washing with ice-cold PBS for three times. Measurement of pyruvate levels from an equal number of cells was performed according to manufacturer's protocol, and normalized to cell number. Acetyl-CoA levels were measured using the PicoProbe Activity Microplate Assay kit (Abcam) in a similar approach, except that protein concentration was used to normalize acetyl-CoA levels. To measure lactate concentration, 24h after transfection, cells were switched to conditional medium (CM) that does not contain phenol red for 24 hours. Lactate levels in CM were then measured using the Lactate Assay kit (Sigma Aldrich). PDH activity was detected by a commercial kit (Sigma Aldrich), following the manufacturer's protocol.

#### **Measurement of lipoprotein lipase (LPL) activity**

Mice were treated with saline, G-control, or G-(P)RR and fed an HFD for 4 weeks. To measure LPL activity, mice were injected with 0.2 U/g heparin via tail-vein, and blood were drawn 15 min after heparin injection. Plasma LPL activity were then measured with a commercial kit from Abcam (catalog nr. ab204721).

#### **Measurement of plasma insulin**

Mice were treated with saline, G-control, or G-(P)RR and fed an HFD for 14 weeks. At 12th week, after 6-hour -fasting, plasma samples were collected and measured for insulin levels with an ultrasensitive mouse insulin ELISA kit from ALPCO (catalog nr. 80-INSMSU-E01), following the standard manufacturer's protocol.

#### **Isolation and culture of primary hepatocytes**

Primary hepatocytes were isolated from C57BL/6J mice using previously described two-step collagenase perfusion method with modifications<sup>13</sup>. Briefly, mice were first perfused with O<sub>2</sub> gassed perfusion buffer (5 mmol/L HEPES, 4 mmol/L KCl, 120 mmol/L NaCl, 1 mmol/L KH<sub>2</sub>PO<sub>4</sub>, 2.4 mmol/L MgSO<sub>4</sub>, 40 mmol/L NaHCO<sub>3</sub>, 20 mmol/L glucose) supplemented with 0.1 mmol/L EDTA, for 5-7 minutes at a constant flow rate at 7 mL/min. Perfusion path was set to flow into liver via inferior vena cava and flow out through portal vein. After the first perfusion step, mice were then perfused with O<sub>2</sub> gassed perfusion buffer supplemented with 2.7 mmol/L CaCl<sub>2</sub> and 1.6 mg/mL Type IV collagenase (Sigma Aldrich, catalog nr. C5138), for 3 -4 minutes at a constant flow rate at 6 mL/min. Primary hepatocytes were released by removing liver capsule, and filtered through 100 µm filtered. Then, primary hepatocytes were washed with ice-cold DMEM and centrifuged at 50x g for 2 min, which was repeated for three times. Primary hepatocytes were seeded at a density of 600,000 cells/well or 8,000 cells/well into collagen coated 6-well plate or Seahorse 24-well plate, respectively, and cultured with DMEM GlutaMax™ high glucose supplemented with

5% FBS. To inhibit (P)RR expression in mouse primary hepatocytes, 0.05 mg/mL G-(P)RR ASO was added to culture medium 3 hours after seeding cells.

### Seahorse XFe24 analyzer

HepG2 cells were seeded to Seahorse 24 -well plate, and cultured with DMEM GlutaMax™ high glucose with 10% FBS. HepG2 cells were transfected with siNC or si(P)RR for 48 hours. Mouse primary hepatocytes were isolated, seeded to Seahorse 24 well plate, and cultured with DMEM GlutaMax™ high glucose supplemented with 5% FBS. To inhibit (P)RR expression, mouse primary hepatocytes were treated with 0.05 µg/mL final concentration of G-(P)RR ASOs for 36 hours. Mitochondrial function and cellular fuel dependency were then measured using Seahorse XF Cell Mito Stress Test Kit and Seahorse XF Mito Fuel Flex Test Kit, following manufacturer's protocol, with the exception that for FA dependency assay oleic acid was added to a final concentration of 50 µmol/L to the cell culture medium 4 hours prior to the start of the assay.

### Immunoblotting

For protein expression and phosphorylation studies, 50 mg mouse liver samples were homogenized in RIPA buffer (50 mM Tris-HCl, 150mM NaCl, 1% Triton X-100, 1% sodium deoxycholate, 0.1% SDS, pH 7.4) with phosphatase inhibitor cocktail (Sigma Aldrich) and protease inhibitors cocktail (Roche) using TissueLyzer (Qiagen). Homogenates were centrifuged at 10,000× g at 4 °C for 10 minutes to clear any cell debris or insoluble proteins. Protein concentrations were then determined using BCA assay (Pierce). Equal amounts of proteins (30-40 mg) were loaded and separated on 4-20% Bis-Tris gels (GenScript), and transferred to PVDF membranes using iBlot® 2 Dry Blotting System (Thermo Fisher Scientific). For high -molecular weight proteins such as acetyl-CoA carboxylase (ACC), samples were loaded and separated on 6% SDS -PAGE gels with ice-cold buffers for 3-5 hours, and transferred to PVDF membranes using traditional wet transferring system at 4 °C for 16 hours. The blots were then probed with the antibodies listed in Online Table I and detected by Clarity™ Western Substrate (Bio-rad). The intensities of bands were analyzed using ImageJ.

**Online Table I. Antibodies used in the study.**

Target	Species originated	Dilution	Source	Catalog number
(P)RR	Rabbit	1: 1000	Sigma	HPA003156
SORT1	Mouse	1: 1000	BD Bioscience	612100
LDLR	Rabbit	1: 1000	Thermo Fisher Scientific	PA5-22976
PDHA	Rabbit	1: 1000	Proteintech	18068-1-AP
PDHB	Rabbit	1: 1000	Proteintech	14744-1-AP

ACC $\alpha$ / $\beta$	Rabbit	1: 1000	Cell Signaling Technology	9957
PPAR $\gamma$	Rabbit	1: 1000	Cell Signaling Technology	2435
Adiponectin	Rabbit	1: 1000	Cell Signaling Technology	2789
$\beta$ -actin	Mouse	1: 3000	Proteintech	60008-1

### RNA isolation and qPCR analysis

Liver samples were homogenized with Trizol (Thermo Fisher Scientific) and total RNA was extracted using Direct-zol<sup>TM</sup> RNA MiniPrep kit (ZYMO Research). One microgram of total RNA was reverse transcribed with Prime Script<sup>TM</sup> RT Master Mix (TaKaRa). SYBR Green real-time quantitative PCR assays were performed on a qTOWER apparatus (Analytic Jena) using SYBR <sup>®</sup>Premix Ex Taq<sup>TM</sup> II kit (TaKaRa). Primers used in the study were listed in Online Table II.

### Hepatic lipids extraction and measurement

To measure hepatic lipid contents, lipids in the liver were extracted using Folch's method<sup>14</sup>. In short, 50 mg liver samples were homogenized using Tissue lyzer (60Hz, 30s) in chloroform and methanol mixture (2:1) followed by adding methanol, chloroform and MQ. Extracted lipids were dried with N<sub>2</sub> gas and dissolved with 200 $\mu$ l PBS containing 1% Triton X-100. Cholesterol, triglycerides and non-esterified fatty acid (NEFA) were measured using colorimetric kits (Wako).

### Statistics

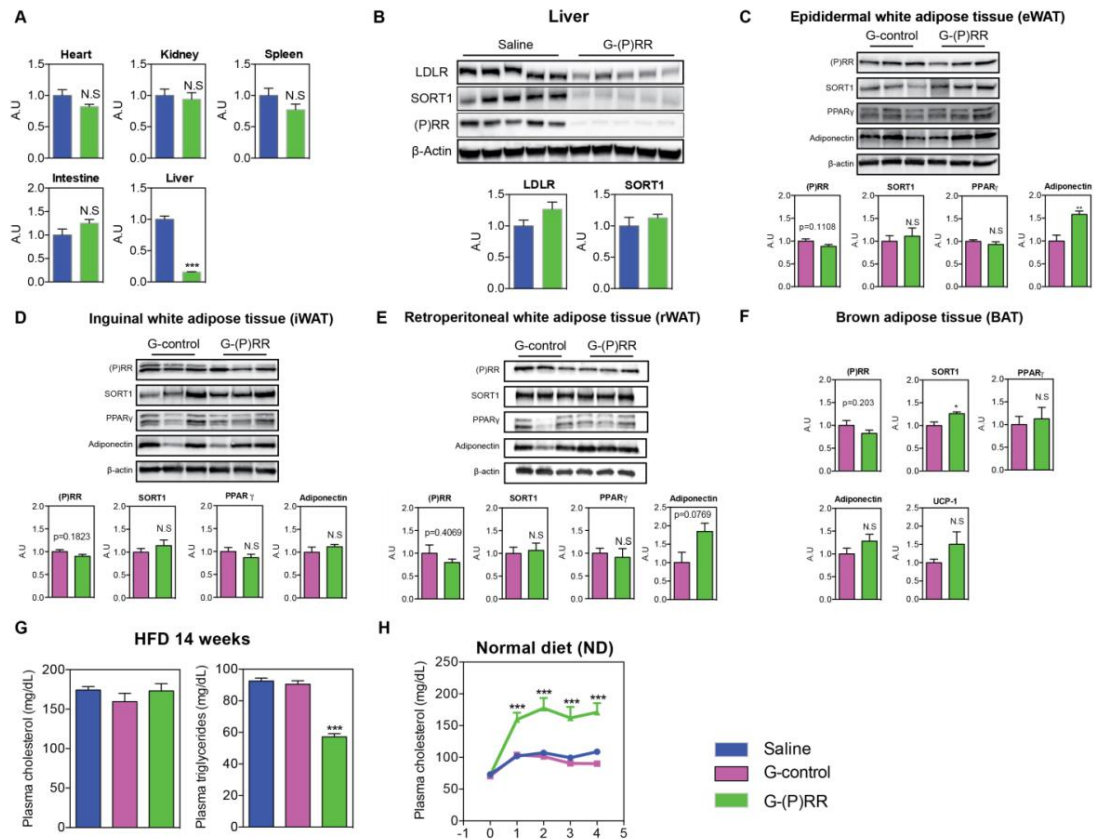
All values were presented as mean  $\pm$  SEM. For experiments with n number  $\geq$  8/group, D'Agostino-Pearson omnibus test was performed to test normality. For experiments with less n number, Kolmogorov -Smirnov test was performed for normality test. After passing normality test, one-way ANOVA followed by the Bonferroni test was performed for comparison of more than two groups. And student t-test was used to compare the differences between two groups. P values of  $<0.05$  were considered significant.

### Online Table II. List of qPCR primer sequences.

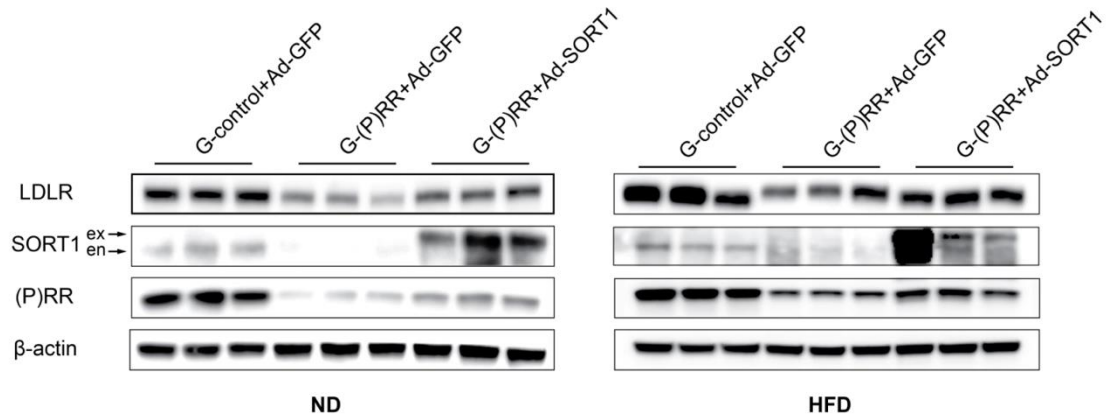
Gene		sequence
(P)RR	Forward	5'-GGGTGGATAAACTGGCACTTC-3'
	Reverse	5'-TGGAATTTGCAACGCTGTC-3'
SORT1	Forward	5'-TGAGGACATGGTCTTCATGC-3'
	Reverse	5'-GGTAAAGATGGTGCCAAACC-3'
LDLR	Forward	5'-GATGGCTATACCTACCCCTCAA-3'
	Reverse	5'-TGCTCATGCCACATCGTC-3'
PDHA	Forward	5'-GGCATCGTTGGAGCTCAG-3'
	Reverse	5'-ACAGACCTCATCTTTTCCATTGT-3'

PDHB	Forward	5'-GAGCTGAGATTTGTGCCAGA-3'
	Reverse	5'-ACATCAGCACCAGTGACACG-3'
ACC $\alpha$	Forward	5'-GGCTCAAACCTGCAGGTATCC-3'
	Reverse	5'-TTGCCAATCCACTCGAAGA-3'
ACC $\beta$	Forward	5'-TGAATCTCACGCGCCTACTA-3'
	Reverse	5'-TTGTGTTCTCGGCCTCTCTT-3'
PPAR $\gamma$	Forward	5'-GAAAGACAACGGACAAATCACC-3'
	Reverse	5'-GGGGGTGATATGTTTGAACCTG-3'
Adiponectin	Forward	5'-GGGGGTGATATGTTTGAACCTG-3'
	Reverse	5'-CTTTCCTGCCAGGGGTTC-3'
UCP-1	Forward	5'-GGCCTCTACGACTCAGTCCA-3'
	Reverse	5'-TAAGCCGGCTGAGATCTTGT-3'
Hadha	Forward	5'-GAAATGGATAATATCTTGGCAAATC-3'
	Reverse	5'-TGGACGTCTTCATCAGAGGAG-3'
Acaa2	Forward	5'-AAATGTGCGCTTCGGAAC-3'
	Reverse	5'-CGTTAATCCTGCCACAAAG-3'
Acadv1	Forward	5'-GGTGGTTTGGGCCTCTCTA-3'
	Reverse	5'-TCCCAGGGTAACGCTAACAC-3'
Acadl	Forward	5'-GCTTATGAATGTGTGCAACTCC-3'
	Reverse	5'-CCGAGCATCCACGTAAGC-3'
$\beta$ -actin	Forward	5'-CTAAGGCCAACCGTGAAAAG-3'
	Reverse	5'-ACCAGAGGCATACAGGGACA-3'

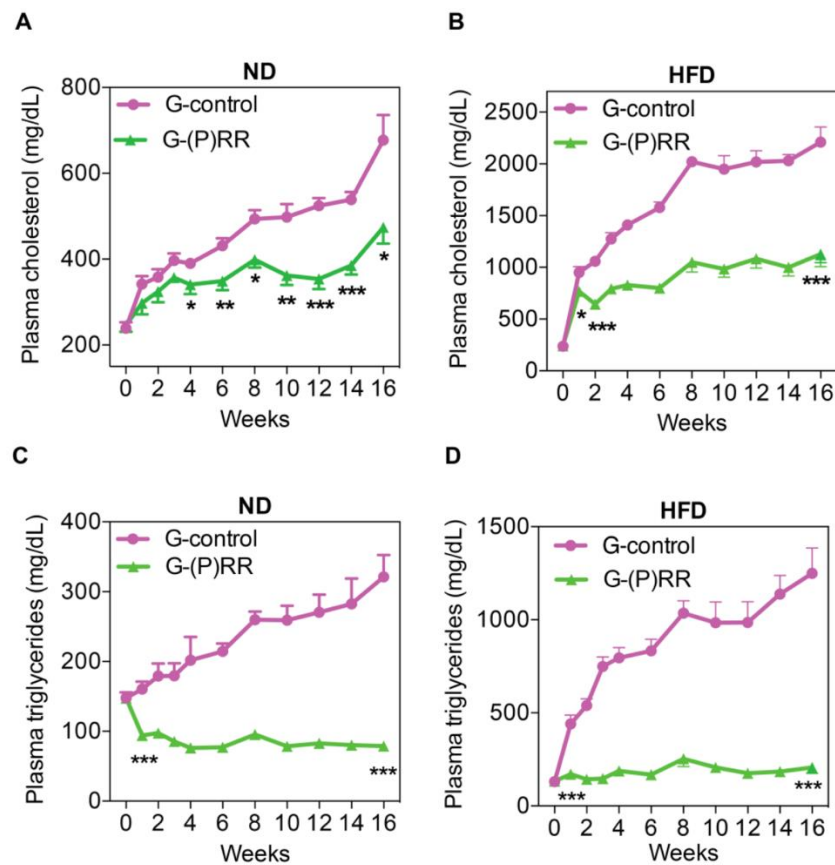
---



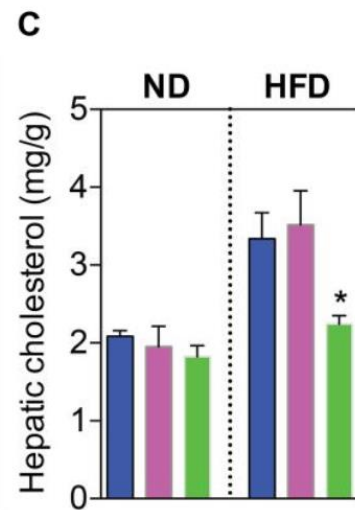
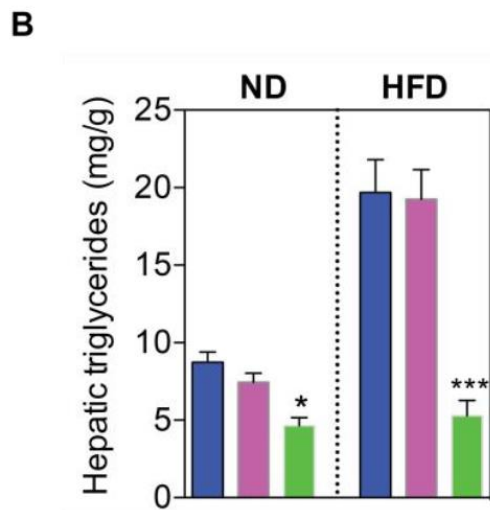
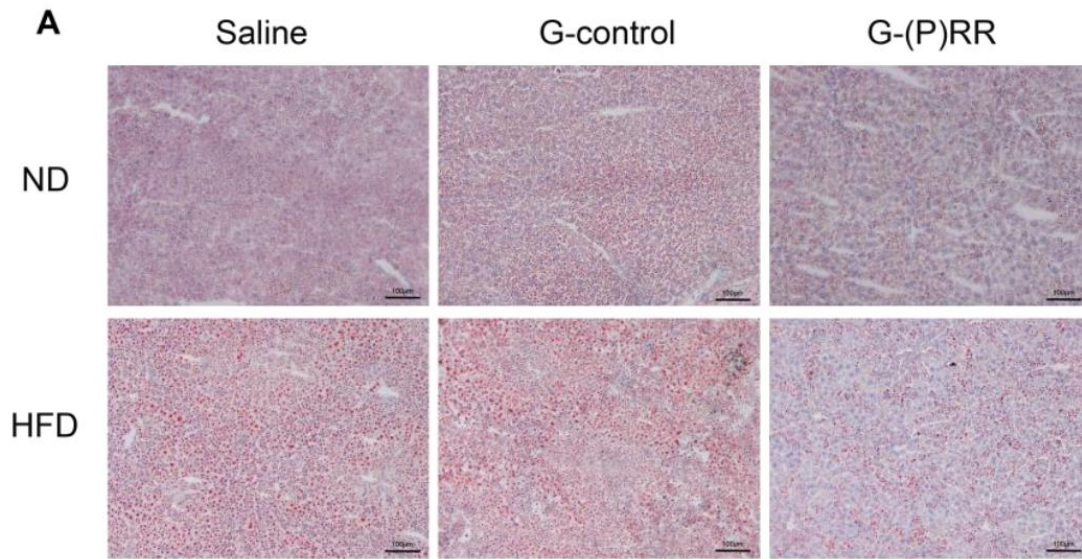
**Online Figure I.** GalNAc-(P)RR ASO specifically targets hepatic (P)RR and affects plasma lipid concentrations. (A) Eight-weeks old male C57BL6 mice were injected with saline (blue) or G-(P)RR (green). After 5 days, mice were sacrificed and tissues were collected and analyzed for (P)RR expression. (P)RR expression was normalized by the geometric mean of the expression of actin, 36B4 and GAPDH. N=5/group; \*\*\*,  $p < 0.001$ . (B) Immunoblotting of liver samples from saline or G-(P)RR treated mice. (C-E) (P)RR expression levels and protein abundance in epididymal white adipose tissue (eWAT), inguinal white adipose tissue (iWAT), and retroperitoneal white adipose tissue (rWAT) of mice treated with G-control or G-(P)RR for 14 weeks and fed with HFD. (F) (P)RR expression in brown adipose tissue (BAT) of mice treated with G-control or G-(P)RR for 14 weeks and fed with HFD. (G) G-(P)RR did not affect mRNA levels of LDLR and SORT1. N=6 per group. (D) Plasma triglycerides and cholesterol concentration of C57BL6 mice injected with saline (blue), G-control (magenta) or G-(P)RR (green), and fed HFD for 14 weeks. N=10 per group. \*\*\*,  $p < 0.001$ . G-control v.s G-(P)RR. (H) Plasma cholesterol levels of C57BL6 mice treated as indicated, and fed ND for 4 weeks. N=12 per group. \*\*\*,  $p < 0.001$ . G-control v.s G-(P)RR.



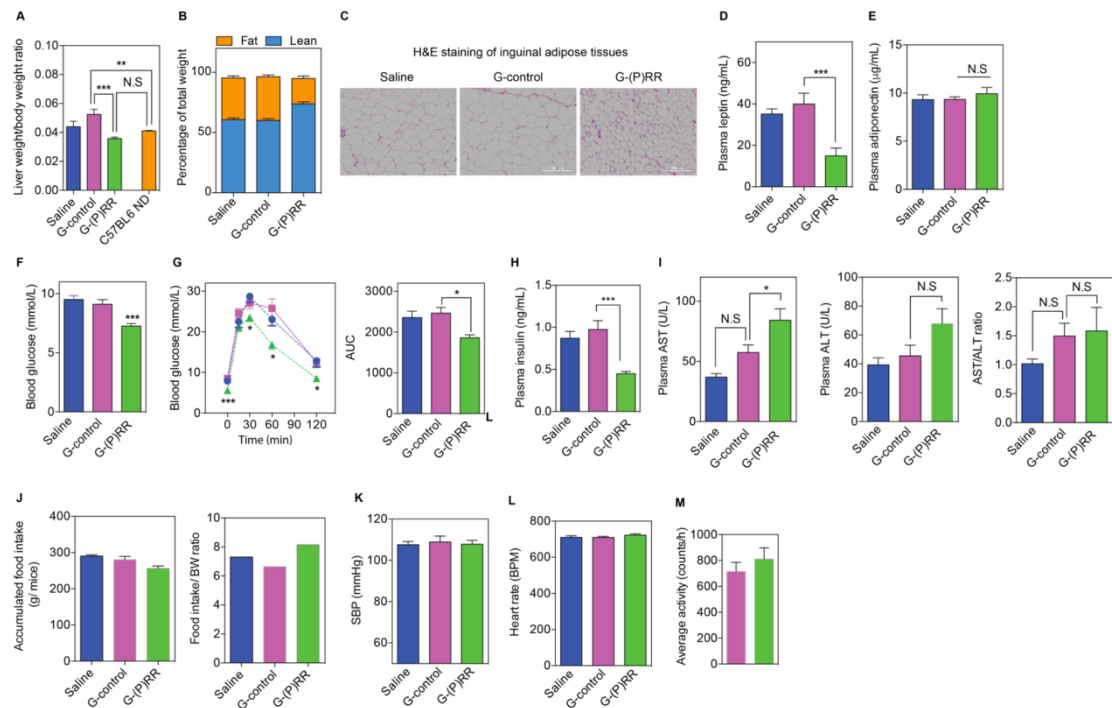
**Online Figure II.** SORT1 overexpression does not prevent PRR deficiency induced reduction in LDLR protein levels in the liver. Eight-week-old male mice were treated with G-control or G-(P)RR, in combination of control adenovirus (Ad-GFP) or SORT1 expressing adenovirus (Ad-SORT1). N=6 per mice. Representative blot. Ex: exogenously expressed hSORT1. En: endogenously expressed mSORT1.



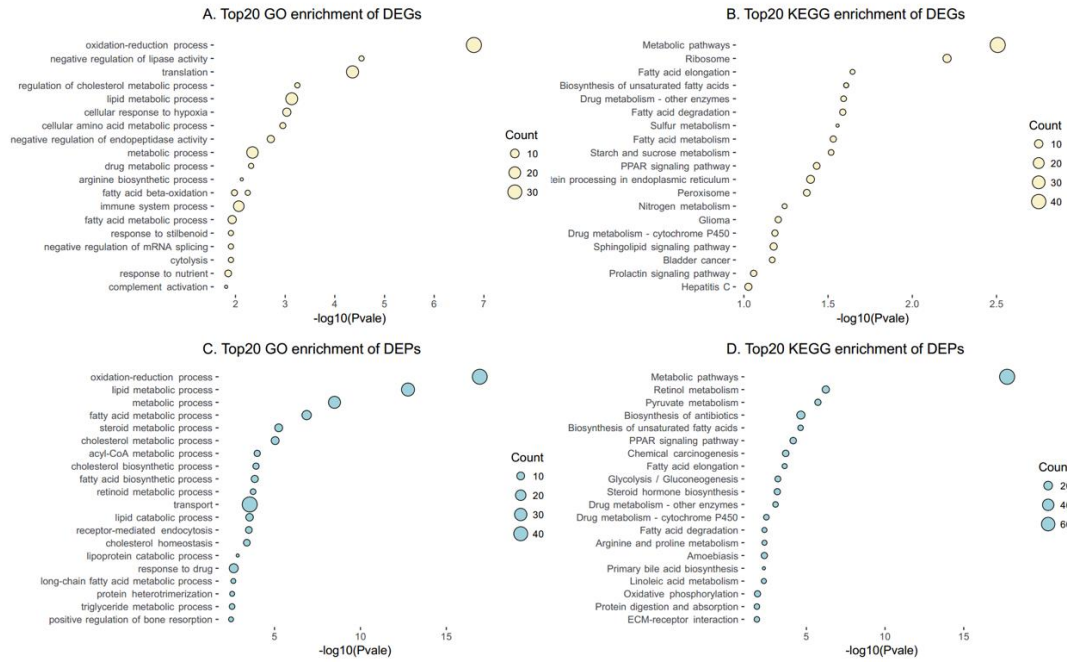
**Online Figure III.** Inhibiting hepatic (P)RR in LDLR<sup>-/-</sup> mice reduces plasma cholesterol and triglyceride levels under both chow and HFD conditions. Eight-week-old male mice were treated with G-control (magenta) or G-(P)RR (green), and fed with ND or HFD for 16 weeks. Plasma cholesterol levels (A&B) and plasma triglyceride levels (C&D) were monitored weekly in the first 4 weeks, and bi-weekly afterwards. N=8 per group. \*: p<0.05; \*\*: p<0.01; \*\*\*: p<0.001.



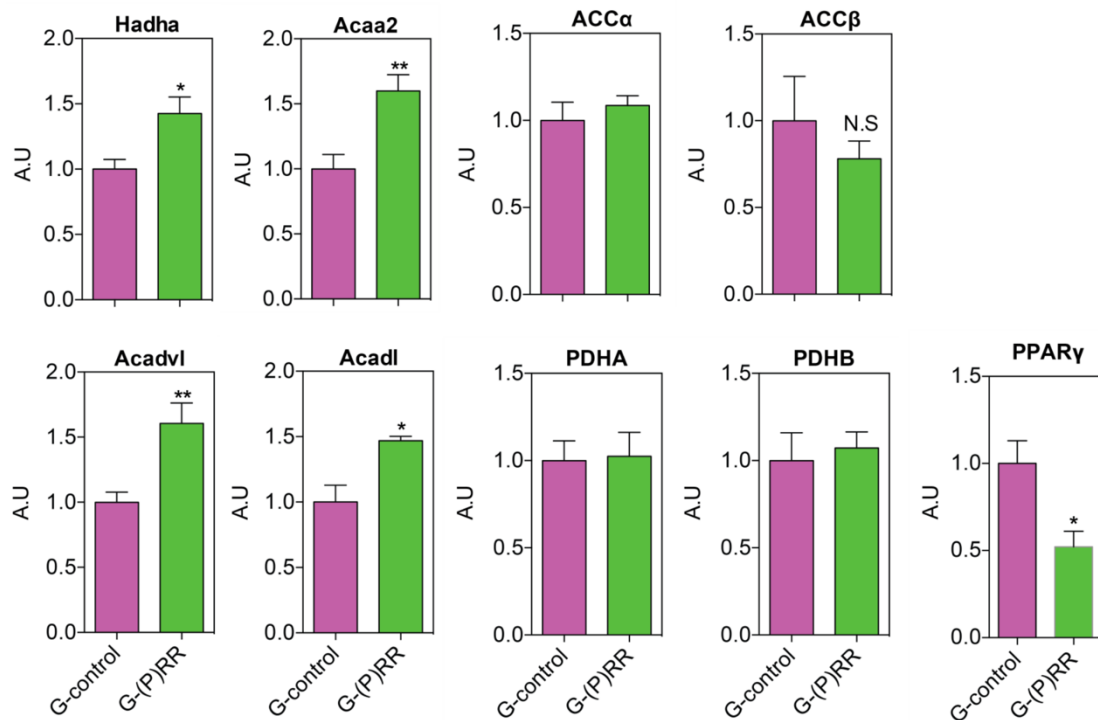
**Online Figure IV.** Inhibiting the (P)RR reduces hepatic lipid levels under both ND and HFD conditions. Eight-week -old male mice were treated with saline (blue), G-control (magenta) or G-(P)RR (green ) for 4 weeks, fed ND or HFD. (A) Representative image of Oil Red O staining of liver samples. (B&C) Lipids were extracted from the liver using Folch's method, and dried with N<sub>2</sub> gas. Resuspended lipids were measured for triglycerides and cholesterol, normalized by the weight of liver samples used for lipid extraction. N=12 per group. \*: p<0.05; \*\*\*: p<0.001.



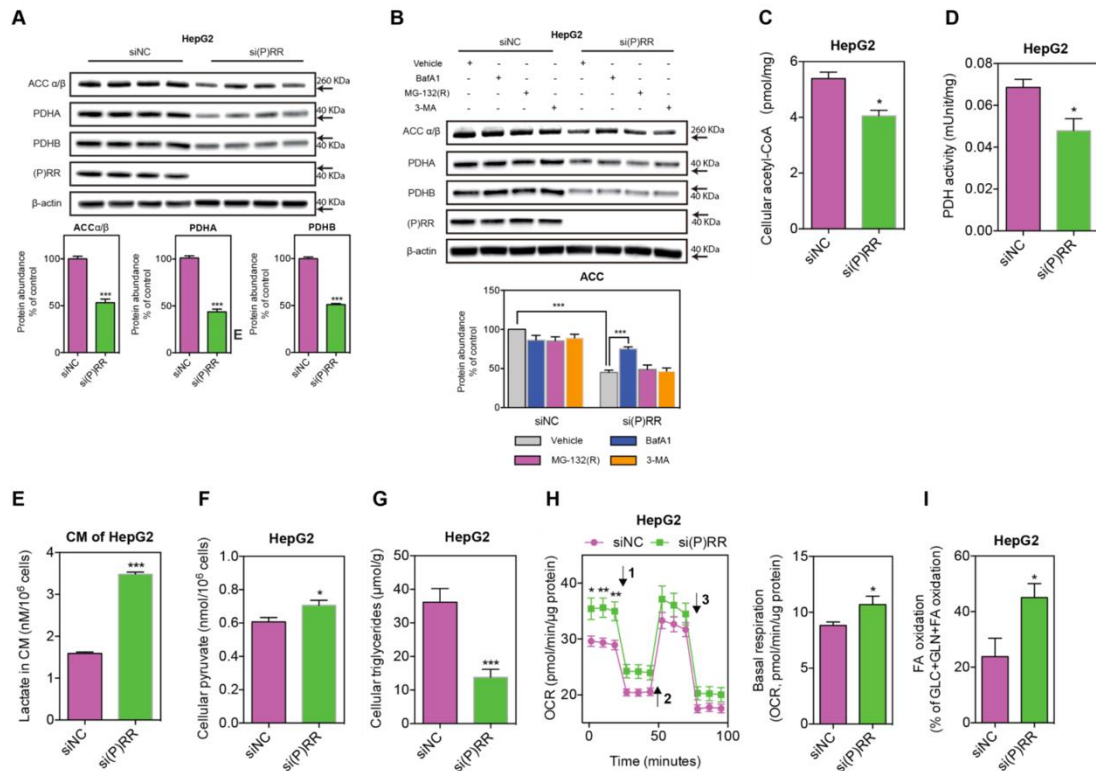
**Online Figure V.** Relevant information of hepatic (P)RR inhibition in C57BL6 mice fed HFD for 14 weeks. Eight-week-old male mice were treated as indicated, and fed HFD for 14 weeks. (A) LW/BW ratio. LW/BW of C57BL6 mice at similar age, fed ND, was used as a reference value (n=6). N=10 per group. \*\*\*:  $p < 0.001$ . (B) Percentage of fat and lean mass of total weight. (C) Representative image of H&E staining of inguinal white adipose tissue. (D) Plasma leptin concentrations. (E) Plasma adiponectin concentrations. (F) Fasting glucose levels of the mice were measured on week 12 of the HFD. (G) Intraperitoneal glucose tolerance test (IPGTT) was performed on week 13 of the HFD. Glucose levels at each time point were compared by One-way ANOVA and \* indicates significant differences between G-control and G-(P)RR injected mice. AUC was used to compare the overall differences between groups. (H) Fasting plasma insulin levels at 12th week. (I) plasma ALT and AST activity, and AST/ALT ratio. N=10 per group; \*:  $p < 0.05$ ; (J) accumulated food intake during experimental period, and accumulated food intake adjusted by end time body weight. SBP (K) and heart rate (L) measured 7 days prior to sacrifice. N=10 per group. (M) 24h average physical activity of G-control injected and G-(P)RR injected mice was monitored with a metabolic monitoring system 4 days prior to sacrifice. N=8 per group.



**Online Figure VI.** GO enrichment analysis reveals that inhibiting the (P)RR extensively affects genes involved in metabolic processes. Analysis of transcriptome (A&B), or comparative proteomics (C&D). Top 20 enriched biological processes (BP) (A&C). Top 20 enriched KEGG pathways (B&D).



**Online Figure VII.** Hepatic genes expression are affected by (P)RR inhibition. Eight-week-old male C57BL6 mice were treated with G-control or G-(P)RR, fed HFD for 14 weeks. Hepatic gene expressions were analyzed, and normalized by the expression of  $\beta$ -actin in the same sample. N=6 per group. \*:  $p<0.05$ ; \*\*:  $p<0.01$ .



**Online Figure VIII.** Silencing the (P)RR in HepG2 cells reduces ACC and PDH protein abundance resulting in increased oxygen consumption and dependency on fatty acid as fuel source. (A) (P)RR expression was silenced in HepG2 cells and a representative blot of 3 independent experiments in quadruplicate is shown. Total cell lysates were immunoblotted as indicated, and the level of PDHA, PDHB, and ACC $\alpha/\beta$  protein was quantified and normalized to the level of  $\beta$ -actin in the same lysate. \*\*\*:  $p < 0.001$ . (B) HepG2 cells were transfected with control or (P)RR siRNAs for 48h. Cells were incubated with vehicle control, 100 nmol/L bafilomycin A1 (BafA1), 7.5 mmol/L 3-3-Methyladenine, and 20  $\mu$ mol/L MG-132(R) for 8 hours. A representative blot of 4 independent experiments and corresponding quantification is shown. (C-G) To measure cellular metabolites, HepG2 cells were transfected with control siRNA (siNC) or siRNA against (P)RR [si(P)RR] for 48 hours. Subsequently, cells or medium were prepared as described to measure intracellular acetyl-CoA levels (C), PDH activity (D), lactate levels in the conditional medium (CM) (E), intracellular pyruvate levels (F), and intracellular triglyceride levels (G). Three independent experiments in triplicate were performed for each measurement and values were corrected with either the amount of protein or number of cells.  $N = 9$  per group; \*:  $p < 0.05$ ; \*\*\*:  $p < 0.001$ . (H-I) Cellular oxygen consumption rates (OCR) (H) and fuel dependency (I) were measured in HepG2 cells treated with siNC or si(P)RR for 48 hours. Arrow 1-3 indicates addition of oligomycin, FCCP and the mixture of rotenone and antimycin, respectively.  $N = 6$  per group. \*:  $p < 0.05$ ; \*\*\*:  $p < 0.01$ .

## References

1. Seth PP, Siwkowski A, Allerson CR, Vasquez G, Lee S, Prakash TP, Kinberger G, Migawa MT, Gaus H, Bhat B, Swayze EE. Design, synthesis and evaluation of constrained methoxyethyl (cmoe) and constrained ethyl (cet) nucleoside analogs. *Nucleic Acids Symp Ser (Oxf)*. 2008;553-554
2. Prakash TP, Yu J, Migawa MT, et al. Comprehensive structure-activity relationship of triantennary n-acetylgalactosamine conjugated antisense oligonucleotides for targeted delivery to hepatocytes. *J Med Chem*. 2016;59:2718-2733
3. Bowe JE, Franklin ZJ, Hauge-Evans AC, King AJ, Persaud SJ, Jones PM. Metabolic phenotyping guidelines: Assessing glucose homeostasis in rodent models. *J Endocrinol*. 2014;222:G13-25
4. Wagschal A, Najafi-Shoushtari SH, Wang L, et al. Genome-wide identification of micrnas regulating cholesterol and triglyceride homeostasis. *Nat Med*. 2015;21:1290-1297
5. Roche-Molina M, Sanz-Rosa D, Cruz FM, Garcia-Prieto J, Lopez S, Abia R, Muriana FJ, Fuster V, Ibanez B, Bernal JA. Induction of sustained hypercholesterolemia by single adeno-associated virus-mediated gene transfer of mutant hpcsk9. *Arterioscler Thromb Vasc Biol*. 2015;35:50-59
6. Franckhauser S, Munoz S, Elias I, Ferre T, Bosch F. Adipose overexpression of phosphoenolpyruvate carboxykinase leads to high susceptibility to diet-induced insulin resistance and obesity. *Diabetes*. 2006;55:273-280
7. Thatcher SE, Zhang X, Howatt DA, Lu H, Gurley SB, Daugherty A, Cassis LA. Angiotensin-converting enzyme 2 deficiency in whole body or bone marrow-derived cells increases atherosclerosis in low-density lipoprotein receptor<sup>-/-</sup> mice. *Arterioscler Thromb Vasc Biol*. 2011;31:758-765
8. Lu H, Howatt DA, Balakrishnan A, Graham MJ, Mullick AE, Daugherty A. Hypercholesterolemia induced by a pcsk9 gain-of-function mutation augments angiotensin ii-induced abdominal aortic aneurysms in c57bl/6 mice-brief report. *Arterioscler Thromb Vasc Biol*. 2016;36:1753-1757
9. Pertea M, Kim D, Pertea GM, Leek JT, Salzberg SL. Transcript-level expression analysis of rna-seq experiments with hisat, stringtie and ballgown. *Nat Protoc*. 2016;11:1650-1667
10. Kim D, Langmead B, Salzberg SL. Hisat: A fast spliced aligner with low memory requirements. *Nat Methods*. 2015;12:357-360
11. Frazee AC, Pertea G, Jaffe AE, Langmead B, Salzberg SL, Leek JT. Ballgown bridges the gap between transcriptome assembly and expression analysis. *Nat Biotechnol*. 2015;33:243-246
12. Huang DW, Sherman BT, Tan Q, Kir J, Liu D, Bryant D, Guo Y, Stephens R, Baseler MW, Lane HC, Lempicki RA. David bioinformatics resources: Expanded annotation database and novel algorithms to better extract biology from large gene lists. *Nucleic Acids Res*. 2007;35:W169-175
13. Severgnini M, Sherman J, Sehgal A, Jayaprakash NK, Aubin J, Wang G, Zhang L, Peng CG, Yucius K, Butler J, Fitzgerald K. A rapid two-step method for isolation of functional primary mouse hepatocytes: Cell characterization and asialoglycoprotein receptor based assay development. *Cytotechnology*. 2012;64:187-195

14. Folch J, Lees M, Sloane Stanley GH. A simple method for the isolation and purification of total lipides from animal tissues. *J Biol Chem.* 1957;226:497-509